



UNIVERSITY OF LEEDS

This is a repository copy of *Groundwater flow velocities in a fractured carbonate aquifer-type: Implications for contaminant transport*.

White Rose Research Online URL for this paper:  
<http://eprints.whiterose.ac.uk/142561/>

Version: Accepted Version

---

**Article:**

Medici, G, West, LJ and Banwart, SA [orcid.org/0000-0001-7223-6678](https://orcid.org/0000-0001-7223-6678) (2019) Groundwater flow velocities in a fractured carbonate aquifer-type: Implications for contaminant transport. *Journal of Contaminant Hydrology*, 222. pp. 1-16. ISSN 1873-6009

<https://doi.org/10.1016/j.jconhyd.2019.02.001>

---

**Reuse**

This article is distributed under the terms of the Creative Commons Attribution-NonCommercial-NoDerivs (CC BY-NC-ND) licence. This licence only allows you to download this work and share it with others as long as you credit the authors, but you can't change the article in any way or use it commercially. More information and the full terms of the licence here: <https://creativecommons.org/licenses/>

**Takedown**

If you consider content in White Rose Research Online to be in breach of UK law, please notify us by emailing [eprints@whiterose.ac.uk](mailto:eprints@whiterose.ac.uk) including the URL of the record and the reason for the withdrawal request.

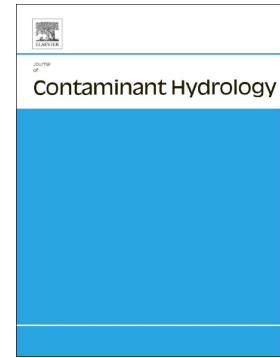


[eprints@whiterose.ac.uk](mailto:eprints@whiterose.ac.uk)  
<https://eprints.whiterose.ac.uk/>

## Accepted Manuscript

Groundwater flow velocities in a fractured carbonate aquifer-type:  
Implications for contaminant transport

G. Medici, L.J. West, S.A. Banwart



PII: S0169-7722(18)30290-0

DOI: <https://doi.org/10.1016/j.jconhyd.2019.02.001>

Reference: CONHYD 3459

To appear in: *Journal of Contaminant Hydrology*

Received date: 22 September 2018

Revised date: 19 January 2019

Accepted date: 1 February 2019

Please cite this article as: G. Medici, L.J. West and S.A. Banwart, Groundwater flow velocities in a fractured carbonate aquifer-type: Implications for contaminant transport, *Journal of Contaminant Hydrology*, <https://doi.org/10.1016/j.jconhyd.2019.02.001>

This is a PDF file of an unedited manuscript that has been accepted for publication. As a service to our customers we are providing this early version of the manuscript. The manuscript will undergo copyediting, typesetting, and review of the resulting proof before it is published in its final form. Please note that during the production process errors may be discovered which could affect the content, and all legal disclaimers that apply to the journal pertain.

## Groundwater flow velocities in a fractured carbonate aquifer-type; implications for contaminant transport

G. Medici<sup>a</sup>, L.J. West<sup>\*a</sup>, S.A.. Banwart<sup>a</sup>

<sup>a</sup> School of Earth and Environment, University of Leeds, Woodhouse Lane, Leeds, W Yorkshire, LS2 9JT, UK

\*Corresponding author at: School of Earth and Environment, University of Leeds, Leeds LS 9TJ, United Kingdom.

E-mail address: L.J.West@leeds.ac.uk (Jared West)

### Abstract

Contaminants that are highly soluble in groundwater are rapidly transported via fractures in mechanically resistant sedimentary rock aquifers. Hence, a rigorous methodology is needed to estimate groundwater flow velocities in such fractured aquifers. Here, we propose an approach using borehole hydraulic testing to compute flow velocities in an un-faulted area of a fractured carbonate aquifer by applying the cubic law to a parallel plate model. The Cadeby Formation (Yorkshire, NE England) – a Permian dolostone aquifer present beneath the University of Leeds Farm - is the fractured aquifer selected for this hydraulic experiment.

The bedding plane fractures of this dolostone aquifer, which are sub-horizontal, sub-parallel and laterally persistent, largely dominate the flow at shallow (<~40 mBGL) depths. These flowing bedding plane discontinuities are separated by a rock matrix which is relatively impermeable ( $K_{well-test}/K_{core-plug} \sim 10^4$ ) as is common in fractured carbonate aquifers.

In the workflow reported here, the number of flowing fractures – mainly bedding plane fractures - intersecting three open monitoring wells are found from temperature/fluid conductivity and acoustic/optical televiewer logging. Following well installation, average fracture hydraulic apertures for screened intervals are found from analysis of slug tests. For the case study aquifer, this workflow predicts hydraulic apertures ranging from 0.10 up to 0.54 mm. However, groundwater flow velocities range within two order of magnitude from 13 up to 242 m/day.

Notably, fracture apertures and flow velocities rapidly reduce with increasing depth below the water table; the upper ~ 10 meters shows relatively high values of

hydraulic conductivity (0.30 - 2.85 m/day) and corresponding flow velocity (33 - 242 m/day). Permeability development around the water table in carbonate aquifer-types is common, and arises where high pCO<sub>2</sub> recharge water from the soil zone causes calcite/dolomite dissolution. Hence, agricultural contaminants entering the aquifer with recharge water are laterally transported rapidly within this upper part.

Computation of groundwater flow velocities allows determination of the Reynolds number. Values of up to ~1, indicating the lower limit of the transition from laminar to turbulent flow, are found at the studied site, which is situated away from major fault traces. Hence, turbulent flow is likely to arise in proximity to tectonic structures, such as normal faults, which localize flow and enhance karstification. The occurrence of turbulent flow in correspondence of such tectonic structures should be represented in regional groundwater flow simulations.

**Keywords:** Carbonate; Fracture; Velocity; Depth; Reynolds number

## 1. Introduction

A range of contaminants reach the saturated part of fractured aquifers in areas of the world which are devoted to agriculture and farming activity, including nitrate, sulphate, chloride and toxic organic compounds released by mineral fertilizers and pesticides, which are highly soluble in groundwater (Foster, 1976; Thorbjarnarson and Mackay, 1997; Danielopol et al., 2013; Meckenstock et al., 2004; Bloomfield et al., 2006; Rivett et al., 2007, 2008; Fouillac et al., 2007; Guy et al., 2009; Lerner and Harris 2009; Stein et al., 2010; Petitta et al., 2009; Stein et al., 2010; Zhang et al., 2013; Re et al., 2017). Additionally, animal excreta represent a further source of nitrate and bacteria from farmland (Conboy and Goss, 2000; Wakida and Lerner, 2005; Rivett et al., 2008; Mellor and Cey, 2015).

Rapid solute transport of contaminants occurs within bedding plane fractures and joints, rather than via the intergranular porosity in most sedimentary rocks (Odling and Roden, 1997; Jourde et al., 2002; Winter et al., 2003; Tellam and Barker, 2006; Cai et al., 2007; Hitchmough et al., 2007; Bailly-Comte et al., 2010; Mondal and Sleep, 2012, 2013; Gellasch et al., 2013; Odling et al., 2013; Tallini et al., 2013; Medici et al., 2016, 2018a, b). Such fractured sedimentary aquifers cover ~55% of the earth's surface being represented in the continental platforms of cratonic areas as well as in more tectonically active sedimentary basins and mountain belts

(Walker, 1967; Blatt et al., 1972; Doglioni, 1994). Hence, contaminant dispersal in groundwater represents a common hazard worldwide due to the growing production of pollutants in areas of intense economic use of land (Berkowitz et al., 1998; Skaggs and Kabala, 1998; Christensen et al., 2000; Thornton et al., 2001).

Fractured carbonate aquifers, which represent the focus of this work, underlie a land area covering ~15% of the earth's surface, supplying ~25% of world population need of drinkable water (Ford and Williams, 1989). Rigorous coupling of hydraulic monitoring (hydraulic head) and field tests (televiwer and/or fluid logs and hydraulic tests) is required to determine parameters (e.g., fracture hydraulic aperture and flow velocity) which control solute transport velocities in their saturated zones.

A methodology for computation of groundwater velocities within fractures has been developed by several authors (Tsang et al., 1990; McKay et al., 1993; Lo et al., 2014; Medici et al., 2016, 2018a; Maldanar et al., 2018; Ren et al., 2018a). Initially, optical and acoustic imaging and fluid logging, or borehole dilution testing are used to determine the number of discontinuities that effectively flow. Next, hydraulic tests on screened intervals are undertaken for computation of fracture permeability and hydraulic aperture using the cubic law. At this stage of the workflow, a large number of authors have derived fracture flow velocities for characterization of fractured igneous and sedimentary aquifers, assuming a parallel plate model of fracture flow (Witherspoon et al., 1980; Li et al., 2008; Quinn et al., 2011). Indeed, application of the cubic law to a parallel plate model is considered reasonable in absence of karstic cavities for fractured aquifers with flow dominated by sub-parallel discontinuities which are separated by an impermeable matrix (Witherspoon et al., 1980; Berkowitz, 2002). This is the approach of our research for determination of groundwater flow velocities and flow regime (laminar or turbulent as indicated by the Reynolds number) within the fault blocks of a fractured aquifer.

In our investigation, groundwater flow velocities within fractures in a carbonate aquifer under natural conditions have been found using optical and acoustic televiwer / fluid logging and slug tests, with focus on variation with respect to depth and seasonality. Our research contrasts with the previous approaches to determine velocities and type of flow regime for groundwater under natural conditions (Cappa et al., 2008; Quinn et al., 2011; Maldaner et al., 2018). Indeed, the focus is on the variation with both depth and time in a specific case of a non-faulted area. We selected a non-faulted block at specific field site, the University of Leeds Farm (Spennings

Farm) in NE England between the cities of Leeds and York (see Fig. 1A-D), to orient future research in terms of hydraulic testing and modelling strategies for fractured aquifers.

The University of Leeds Farm is an experimental site dedicated to the Critical Zone, which is defined as the outer layer of earth's surface extending from the top of the vegetation cover down to the depth of fresh water circulation in the subsurface (Anderson et al., 2008). Research at this experimental site is focused on the migration of the impact of human activities, specifically agriculture in this case, on this outer layer which is of paramount importance for both human health and economic development (Banwart et al., 2011, 2012).

In this paper, we report a hydro-geophysical characterization of the Critical Zone of the carbonate aquifer of the Permian Magnesian Limestone in Yorkshire (NE England, UK) at the University of Leeds Farm. This experimental farm site (see Fig. 1A-B) is underlain by this dolomitic aquifer and provides an opportunity to assess risk of contaminant transport in an area of the UK which is characterized by intense agricultural and farming activity. In fact, 80% of NE England is arable and livestock farmland; as a result the concentration of nitrates in groundwater has steadily increased since 1940 due to introduction of nitrogen fertilizers (Foster et al., 1982; Adams et al., 2006). Previous research describes the Magnesian Limestone Group as a carbonate aquifer where flow is largely dominated by fractures (Cairney, 1972; Allen et al., 1997). Hence, the site at the University of Leeds Farm is an optimum laboratory to investigate fracture flow in an area where hazards from contaminant dispersal is relatively high (Foster and Crease, 1974; Foster et al., 1982).

Previous published studies on the hydraulic properties of the Magnesian Limestone aquifer in NE England have focused on core plug and pumping test analyses and hydro-geochemistry (Cairney, 1972; Aldrick, 1978; Younger, 1995; Allen et al., 1997; Mayes et al., 2005). More recently, a steady state groundwater flow model was published for an area further north in County Durham (Fig. 1B; Neymeyer et al., 2007). Here, we propose an investigation using a combination of experimental techniques including fracture analysis on optical and televiewer logs, monitoring of the water table, slug tests and temperature and electrical conductivity fluid logs, new to this aquifer.

Specific research objectives are as follows: (i) estimate hydraulic conductivities and hence apertures of flowing discontinuities, (ii) estimate groundwater velocities and

Reynolds number and their variation with depth and time, and (iii) address future research needs for carbonate aquifer-types.

## **2 Study area**

### *2.1 Geological setting*

The Magnesian Limestone aquifer is characterized by carbonate rocks derived from shallow water sedimentation at the margins of the Zechstein Basin (Aldrick, 1978; Lee, 1993). In NE England, the Magnesian Limestone aquifer attains a typical thickness of 120 m (Fig. 1A-D) and is formally part of the Zechstein Group, which is characterized by a succession of marine dolomite, limestone, evaporites, mudstone and siltstone of exclusively Permian age (Smith et al. 1986; Tucker, 1991). The Magnesian Limestone Group is formally divided into three different formations: the Cadeby, Edlington and Brotherton formations (Fig. 1B; Smith et al., 1986).

The Cadeby and Brotherton formations represent the mainly carbonate units; they are separated by the marls, mudstones and evaporites of the Edlington Formation. The base of the Cadeby Formation is characterized by 5 meters of marls which separate the aquifer from the sandstone, mudstone and clays of the Pennines Coal Measures Group (Fig. 1B, C). The Brotherton Formation passes upwards into the Roxby Formation which is entirely characterized by anhydrite and gypsum (Allen et al., 1997).

The Cadeby Formation is characterized, with the exception of the basal 5 meters of marls, by thinly bedded dolostone showing ooids, corals and bivalves (Tucker, 1991). This formation, which represents the focus of this study, was deposited during the Lower Permian (272-251 Ma) in a shallow marine environment under sub-tropical climatic conditions. Then, secondary dolomitization occurred at early (Permian) and middle (Triassic) diagenetic stages (Peryt and Sholle, 1996). Dolomitization fluids were supplied from the gypsum and evaporites of the overlying Edlington Formation (Smith et al., 1986). The Brotherton Formation above represents the uppermost part of the Magnesian Limestone aquifer in Yorkshire and is characterized by thinly bedded dolomitic limestone with ooids, algae and bivalves. The Brotherton Formation was also deposited in a shallow water environment under tropical conditions; but it differs from the Cadeby Formation due to less intense dolomitization (Peryt and Sholle, 1996).

In NE England around the University of Leeds Farm (Fig. 1B, D), the tectonic structures which characterize the UK Magnesian Limestone aquifer are represented by normal faults and non-stratabound joints (*sensu* Hartmann et al., 2007). Outcrop studies and seismic lines carried out near the field site show how normal faults of Mesozoic age are mainly oriented ENE-SSW (Fig. 1B; Aitkenhead, 2002, Cooper and Lawley, 2007; Medici et al., 2015). The Cenozoic Alpine orogenesis results in the gentle dip ( $< 5^\circ$  towards E) of the Permo-Mesozoic deposits in the Yorkshire area (Fig. 1B, C; Bottrell et al., 2006; Hartmann et al., 2007; Bricker et al., 2012). Outcrop observations of the Cadeby and Botherton formations show how normal faults represent areas of high fracture density (Aldrick, 1978). However, non-faulted sections in Highmoor Quarry at the University of Leeds Farm site (Fig 1D) and elsewhere show high angle (dip  $50^\circ$ - $80^\circ$ ) joints of  $\sim 1$ - $2$  m persistence cross-cutting bedding parallel fractures (Fig. 2; Walker, 2006; Boddy, 2018). Such high angle joints have been previously mapped in the Magnesian Limestone aquifer in Yorkshire (Kortas and Younger, 2013). These fractures arise from the Cenozoic uplift of NW Europe and are related to unloading due to removal of overlying strata (Odling et al., 1999; Kortas and Younger, 2013). Other discontinuities that characterize the Magnesian Limestone include sub-horizontal bedding plane fractures and stylolites. Bedding plane fractures in this aquifer are considered beds that have been reactivated by the Cenozoic uplift (Kortas and Younger, 2013). However, stylolites (Figs. 2A, B) represent pressure solution structures that formed during burial diagenesis. Bedding plane fractures exceed the outcrop scale ( $\sim 20$  m) and are much more persistent than stylolites, which in the Cadeby Formation show persistence ranging from 0.5 up to 1.5 m (Fig. 2A; Walker, 2006; Gillham, 2017).

## 2.2 Hydrogeological background

The Magnesian Limestone aquifer represents the fifth and the third most important aquifer in terms of abstraction volume in the entire UK, and NE England, respectively (Cairney, 1972; Allen et al., 1997; Abesser and Lewis, 2015). Contamination in this carbonate aquifer has arisen from the use of fertilizers in agriculture; nitrate concentrations in groundwater rose from average values of 0.28 mg/L to 75 mg/L between 1948 and 2006 in the study area (Aldrick, 1978; Walker, 2006). At the University of Leeds Farm (Fig. 1A-D) the Magnesian Limestone aquifer is unconfined due to absence or presence of only  $\sim 1$  m thick Quaternary cover (Gaunt et al., 1970;

Aldrick, 1978). The Cadeby and Brotherton formations represent aquifers, separated by the Edlington Formation, which is considered a 'leaky' aquitard. Hydraulic connectivity between the two separate formations is either related to faulting or gypsum dissolution that has resulted in the collapse of strata in the Edlington Formation (Farrant and Cooper, 2008).

The Magnesian Limestone Group is typically highly mechanically resistant (UCS of 48 - 75 MPa); it has been used as a building stone in NE England since Roman times (Lott and Richardson, 1997; Lott 2013). In fact, Highmoor Quarry near the study site is one of the few main sources of dimension stone of this lithology, which is elsewhere typically heavily fractured in outcrop (Walker, 2006).

Groundwater flow is directed towards the east driven by topography which is characterized by higher elevations in the adjacent area of Coal Measures strata outcropping to the west (Fig. 1C). The Cadeby Formation interquartile interval ranges for intergranular hydraulic conductivity and porosity are  $2.9 \times 10^{-4}$  to  $0.9 \times 10^{-3}$  m/day and 8.5 to 18.7%, respectively. These ranges substantially overlap those of the Brotherton Formation, which range from  $4.0 \times 10^{-4}$  to  $1.5 \times 10^{-3}$  m/day and 9.9 to 19.0% for intergranular hydraulic conductivity and porosity, respectively (Allen et al., 1997).

Pumping test values from the UK Magnesian Limestone aquifer are reported by Allen et al. (1997); transmissivities range from 6 to 4300 m<sup>2</sup>/day with median of 299 m<sup>2</sup>/day. These pumping tests highlight a lower transmissivity of the Cadeby Formation ( $T_{\text{median}} = 163$  m<sup>2</sup>/day; n=16) with respect to the Brotherton Formation ( $T_{\text{median}} = 420$  m<sup>2</sup>/day; n=15). This has been interpreted as resulting from the higher dolomitisation which characterizes the Cadeby Formation (54% CaCO<sub>3</sub>; 46% MgCO<sub>3</sub>); this reduces the rate of dissolution in correspondence of fractures. By contrast, the dolomitic limestone of the Brotherton Formation is more abundant in calcite (65% CaCO<sub>3</sub>; 35% MgCO<sub>3</sub>), hence more prone to dissolution and permeability development (Allen et al., 1997; Lott and Cooper, 2005).

However, the highest transmissivities in the Magnesian Limestone ( $T_{\text{median}} = 2000$  m<sup>2</sup>/day; n=7) are associated with fault zones due to the high degree of fracturing (Allen et al., 1997; Cooper and Lawley, 2007). The transmissivities within fault blocks are generally lower but extremely variable depending on fracturing density and proximity to rivers (Allen et al., 1997). Flow occurs essentially in correspondence of fractures, i.e. evidenced by the large difference between permeability from pumping

and core plug tests ( $K_{well-test}/K_{core-plug} \sim 10^4$ ; Allen et al. 1997). Scanline surveys which have been carried out in the quarries nearby the field site indicate development of fissures of a few centimetres aperture exclusively in correspondence of extensional faults (Walker, 2006). Water geochemistry in the Cadeby Formation in the area of Durham (Fig. 1A) shows relatively high alkalinity (380-450 mgL<sup>-1</sup>), and relatively high concentrations of sulphate and chloride from dissolution of halite and gypsum from the overlying Edlington Formation (Younger, 1995; Mayes et al., 2005).

### 3 Experimental methods

Three wells (BH1, BH2, BH3) were drilled in the lower part of the Magnesian Limestone aquifer, which is represented by the Cadeby Formation (NE England, UK) at the University of Leeds Farm (Fig. 1A, B). The three wells (30 to 40 m depth) are located within fault blocks avoiding known fault traces. The layout design approximates an equilateral triangle configuration as illustrated in Figure 1D. The boreholes were drilled with diameters ranging from 0.23 and 0.28 m to install a maximum of three piezometer tubes, each with a 0.08 m diameter with screen length ranging from 2.3 to 3.0 m (see construction details in Table. 1).

#### 3.1 Optical and acoustic televiewer logging

Optical and acoustic televiewer (Mount Sopris ALT QL40 mk5) logs were recorded in open boreholes prior to piezometer installation, and the data were analysed by structure picking (*sensu* Williams and Johnson, 2004) of discontinuities. This structure picking allowed stereographic plotting of discontinuities (n=264) as well as the computation of mean vector statistics for each group of fractures using the Stereonet 9 software package (Allmendinger et al., 2012). Discontinuities recorded in logs in the Cadeby Formation have been divided into four groups: bedding plane fractures (D1), stylolites (D2) and SE (D3) and NW (D4) dipping high angle joints.

#### 3.2 Fluid temperature and conductivity logs

Fluid temperature and electrical conductivity logs have been recorded in the three open boreholes using a Geovista mk2 multi-parameter probe. Measurements of fluid temperature and electrical conductivity were undertaken under ambient conditions. Flow logging was realised prior to installation of piezometer tubes in order to define sections dominated by flowing fractures for location of screened intervals

(construction details in Table 1). Boreholes were logged both downwards and upwards but the downward fluid logs are presented here, as these have better data quality.

### *3.3 Slug tests*

Three slug tests have been performed in each of the screened intervals of BH1, BH2 and BH3 boreholes (Tab. 1) using 5, 2 and 5 litres as withdrawal volume following Butler (1998). A Solinst Levellogger Edge 3001 data logger was used to measure hydraulic head variations. A preliminary slug test was carried out in each screened interval to estimate the return time of the initial displacement to 5% of rest water level. Based on this preliminary test, time intervals between the slugs were fixed to 10 minutes for BH1 and BH2. However, a longer period of 30 minutes was used for BH3.

Slug tests analyses in BH1, BH2 and BH3 have been realized using the AquiferWin32 software package. Horizontal hydraulic conductivity ( $K_h$ ) has been computed for each slug ( $n=24$ ) using the methods of Bouwer and Rice (1976) and KGS (1985) applicable to partially penetrating wells in unconfined aquifers.

### *3.4 Hydraulic head monitoring and determination of groundwater flow vector*

Hydraulic gradient and direction of the groundwater flow have been estimated by hydraulic head monitoring in each piezometer from 1<sup>st</sup> October, 2017 to 30<sup>th</sup> June 2018 using a sampling frequency of 1 hour, correcting for barometric pressure variations. Position and elevation of the top of the wells (see Tab. 1) were surveyed with a Leica GPS TS15 device for accurate determination of hydraulic gradient. The accuracy of this GPS device is +/- 10 mm and +/- 20 mm for lateral and vertical position, respectively.

The water table was assumed as planar and the three point estimation method has been used for determination of the groundwater flow vector. The arithmetic averages of the piezometers heads in each borehole were used as variations between piezometers within the same borehole, i.e. differences in head are  $\leq 0.5$  mm. Hourly data of hydraulic gradient magnitude and azimuth of groundwater flow have been calculated with the 3PE Spreadsheet (Beljin et al., 2014).

### 3.5. Potential recharge

Potential recharge ( $R$ ) is defined as the difference between total precipitation ( $P$ ) and the potential evapotranspiration ( $ET_0$ ). Daily totals of rainfall ( $P$ ) are available at the field site, i.e. a rain gauge is installed at the National Centre for Atmospheric Science (NCAS) weather station (see location of the station with respect to BH1, BH2 and BH3 wells in Fig. 1D). Air temperature is also recorded every 30 minutes at this weather station. This allowed computation of potential evapotranspiration ( $ET_0$ ) using the Hargreaves Equation (1),

$$(1) \quad ET_0 = 0.0023R_a(T_m + 17.8)\sqrt{TR},$$

where  $R_a$  is extraterrestrial radiation,  $T_m$  is the daily mean air temperature, computed as an average of the maximum and minimum air temperatures,  $TR$  is the temperature range between minimum and maximum values. Extra-terrestrial radiation,  $R_a$ , is computed using HYDRUS-1D from the latitude and altitude of the field site.

### 3.6. Hydraulic aperture determination

Average fracture hydraulic aperture has been found in order to determine the average groundwater flow velocities in fractures intersecting each screened interval. The hydraulic aperture ( $b$ ) represents the aperture of a parallel walled fracture of equivalent permeability. This hydraulic aperture is expressed by Equation (2) based on the implementation of the cubic law assuming laminar flow (Romm, 1966),

$$(2) \quad b = \sqrt[3]{\frac{12vT_s}{gN}},$$

where  $T_s$  is the screened interval transmissivity,  $g$  is the gravitational acceleration,  $v$  the kinematic viscosity of water ( $1.307 \times 10^{-6}$  m<sup>2</sup>/sec based on the 9.5° fluid temperature at the three boreholes) and  $N$  the number of flowing fractures intersecting the screened interval. Flow in fractures intersecting each screened interval is considered bed-parallel and sub-horizontal as around 90% of flowing fractures are bedding plane fractures with  $< 4^\circ$  dip (see section 4.2 below). Screened

interval transmissivity ( $T_s$ ) is the product of the hydraulic conductivity ( $K_h$ ) from slug tests and the piezometer screen length ( $w$ ). Equation (2) is commonly used for computation of the hydraulic aperture in both fractured carbonate and crystalline aquifers at depths  $< \sim 50$  mBGL (Quinn et al., 2011; Ren et al., 2018a).

### 3.7. Computation of groundwater fracture velocity and flow regime

Average horizontal flow velocity ( $V$ ) in fractures intersecting each of the studied screened intervals can be computed using Equation (3) which is derived from the cubic law assuming fractures as parallel plates (Snow, 1975; Romm, 1966; Qian et al., 2011).

$$(3) \quad V = \frac{b^2 g}{12\nu} i,$$

where  $b$  is the average hydraulic aperture,  $g$  is the acceleration due to gravity,  $\nu$  is the kinematic viscosity of water and  $i$  is the hydraulic gradient along the fracture direction. Here, the average velocity ( $V$ ) in fractures was computed for each screened interval after determination of the hydraulic aperture ( $b$ ) using equation (2) from slug tests, and the hydraulic gradient from the groundwater flow vector (see Section 3.4).

After determination of flow velocity at each screened interval the Reynolds ( $Re$ ) number was found using equation (4) to assess whether laminar or turbulent flow occurs under natural conditions (Ji et al., 2008; Ji and Koh, 2015; Ren et al., 2018a). Reynolds numbers  $< 1$  indicate laminar flow,  $1 - 10$  transitional and  $> 10$  turbulent flow, i.e. laboratory experiments with single fracture models indicate that non-Darcian flow is significant with  $Re$  greater than 1-10 (Witherspoon et al., 1980; Zimmerman et al., 2004; Ranjith and Darlington, 2007; Ji et al., 2008),

$$(4) \quad Re = \frac{V b}{\nu}$$

## 4. Results and Discussion

### 4.1. Aquifer fractures

Outcrop observations at Highmoor Quarry (see Fig. 2) show how the dolomite aquifer of the Cadeby Formation is thinly bedded, i.e. the typical vertical spacing of

bedding planes is 0.4 m in quarry faces. High angle joints ( $50^{\circ}$  -  $80^{\circ}$ ) form a non-stratabound fracturing system, i.e. they typically cross-cut the bedding planes (Fig. 2A). The fracturing network in the three boreholes is representative of a similar non-faulted area. Optical and acoustic televiwer logs do not show displacement of bedding planes or presence of cataclasites confirming the validity of previous geological surveys at the field site (see Fig. 1D).

Good quality optical and acoustic televiwer logs (see Fig. 3) in the three studied wells allowed the structure picking of discontinuities, which are represented by bedding plane fractures (D1), stylolites (D2) and sub-vertical joints (D3, D4), see Figure 4. Low values of amplitude and travel time in acoustic televiwer logs show where bedding plane fractures (D1) and joints (D3, D4) are open, hence representing potential flow pathways (Figs 3A, B, D). Here, optical and acoustic televiwer images show no large ( $>1.5$  mm) karstic features in correspondence of bedding plane fractures and joints (Figs. 3A, B, D). Stylolites (D2) are typically sub-horizontal like the bedding plane fractures (Fig. 2A, B). Despite this, they can be recognized in outcrop and optical and acoustic televiwer logs due to their typical irregular shape (Figs. 2B, 3C; Park and Shot, 1968; Rolland et al., 2014). Acoustic televiwer logs also show how stylolites are characterized by lack of travel time anomalies. Thus, such discontinuities are substantially closed and likely uncondusive for flow.

The optical and acoustic televiwer logs acquired from the three wells confirm that the characteristics of the Cadeby Formation observed in outcrop are also present in the subsurface. The three vertical boreholes show a layered aquifer; 92% of discontinuities are sub-horizontal ( $<30^{\circ}$ ). As a consequence, relatively high angle ( $50^{\circ}$ - $80^{\circ}$ ) fractures characterize only 8% of total discontinuities. However, note that moderate and high angle joints are under-sampled in vertical boreholes. The Terzaghi (1965) correction has been applied in contouring to correct for bias due to the vertical orientation of the three studied boreholes.

Discontinuities grouped in three different families (D1, D2, D3, D4) are plotted as poles in Figure 4A. D1 represents bedding planes, which gently dip towards east (Fig. 4B; mean vector dip azimuth  $=97.5^{\circ}$ ; mean vector dip angle  $= 1.5^{\circ}$ ; vector magnitude  $=0.98$ ;  $n = 192$ ) as common in the Permo-Mesozoic successions of NE England (Fig. 1C; West and Truss, 2006; Odling et al., 2013).

Log discontinuity data (3A, B, D) show a similar vertical spacing (Tab. 2; average vertical spacing = 0.34 m;  $\sigma$  = 0.52 m) to outcrop observations in Highmoor quarry for bedding planes (Fig. 2A). Stylolites (D2) show a very similar orientation (Fig. 4; mean vector dip azimuth = 68.8°; mean vector dip angle = 5.5°; vector magnitude = 0.98; n = 55) with respect to bedding plane fractures (D1), i.e. they form perpendicular to the burial surface by pressure solution processes (Pack and Shot, 1968; Guzzetta, 1984). Stylolites show a higher and more irregular vertical spacing with respect to bedding plane fractures (Tab. 2).

Sub-vertical joints recognized in the three boreholes have been divided into two different families; D3 and D4. High angle (50°-80°) joints dip both towards SE (D3; mean vector dip azimuth = 147.0°; mean vector dip angle = 58.2°; vector magnitude = 0.92; n = 9) and NW (D4; mean vector dip azimuth = 329.0°; mean vector dip angle = 56.8°; vector magnitude = 0.87; n = 8) as illustrated in the stereonet plots in Figure 4. Such high angle joints (Fig. 3A) occur in boreholes with a vertical spacing of 7.0 and 8.5 m for D3 and D4 families, respectively (Tab. 2).

#### 4.2 Fluid logs

Fluid temperature and electrical conductivity have been logged under ambient conditions in all three wells BH1, BH2, BH3 (Fig. 1D, Figs. 5; S1). Fluid temperature ranges from 9.2° up to 10.0°; the vertical profiles do not increase with depth showing lack of correlation with the geothermal gradient. Fluid electrical conductivity shows values up to 110 mS/m (Figs S1, 5); relatively high for potable waters. These values arise from natural alkalinity from carbonate dissolution but also gypsum and halite dissolution in the overlying Edlington Formation; ions flow into the underlying Cadeby Formation through normal faults which juxtapose the two geological formations in the field site area (Fig. 1C; Aldrick, 1978; Mayes et al., 2005).

The three logged boreholes show several inflow horizons identified by changes in gradient in fluid temperature and electrical conductivity in correspondence with visible traces in the optical and acoustic logs (Figs. 5, S1). The number of inflows identified are 5, 7 and 6 for BH1, BH2 and BH3 boreholes, respectively. Each inflow horizon is either characterized by single bedding plane fracture or by a cluster of 2-3 discontinuities which are vertically spaced < 0.10 m.

Effective flowing fractures represent between 30% and 100% of the visible features on the optical and acoustic logs sections corresponding to each screened interval

(Tab. 3). The principal flow pathways in the Magnesian Limestone aquifer are represented by the bedding plane fractures (D1) such as those represented in Figure 3. Indeed, sixteen of the eighteen inflows identified in the three boreholes (BH1 and BH2, BH3) are characterized by bedding plane (D1) discontinuities; nearly all such inflow points are either represented by a single major bedding plane discontinuity (Fig. 3B) or a cluster of minor bedding plane fractures (Fig. 3D). Another, single inflow in BH2 corresponds with two high angle joints (D4); one inflow occurring in BH3 corresponds with both a low angle bedding plane fracture (D1) and a high angle joint (D2). Thus, 90% of the total flowing fractures ( $n=28$ ; Fig. 3) are bedding plane fractures with  $< 4^\circ$  dip. Although high angle joints (Fig. 3A) do not represent the principal flowing structures in the aquifer of the Cadeby Formation, our data indicate they are capable of flow, hence establishing vertical hydraulic connections between bedding plane fractures. No inflows are localised in correspondence of stylolites (D2). To summarise: flow in the Cadeby Formation is largely dominated by bedding plane fractures (D1), sub-vertical joints (D3, D4) secondarily contribute and stylolites (D2) seem to be non-conductive.

#### 4.3 Hydraulic conductivity

Horizontal hydraulic conductivity ( $K_h$ ) values from slug tests are summarized in Table S1 and range from 0.07 to 2.85 m/day showing medians of 0.49 and 0.57 m/day computed using the Bouwer and Rice (1976) and KGS (1985) methodologies, respectively. Comparison of hydraulic conductivities reported in Table S1 indicates that values analysed with Bouwer and Rice (1976) are 2% to 23% lower than those obtained using the KGS (1985)<sup>1</sup>. The latter method has been selected for computation of hydraulic aperture, i.e. specifically developed for fractured anisotropic aquifers (Hyder and Butler, 1995). This fits our hydraulic characterization of the Cadeby Formation, i.e. temperature and electrical conductivity logs show how sub-horizontal bedding plane fractures largely dominate flow.

Hydraulic conductivity computed both using Bouwer and Rice (1976) and KGS (1985) techniques progressively decrease with depth moving from shallower to the deeper screened intervals in all three boreholes. This hydraulic conductivity

---

<sup>1</sup> Note that a number of authors (Hyder and Butler, 1995; Butler, 1998; Cheong et al. 2008) state that assumption of isotropic conditions in the Bouwer and Rice method results in an underestimation of hydraulic conductivity of up to 40% in strongly anisotropic aquifers.

decrease has been plotted in Figure 6 which reports the KGS (1985) values as arithmetic means of the tests in each screened interval.

These screened intervals (BH1 P1, P2; BH2 P1-3; BH3 P1-3) show length ranging from 2.3 up to 3.0 meters and are characterized by a similar number ( $n = 2-5$ ) of sub-horizontal bedding plane fractures (D1). Such sub-horizontal discontinuities represent the principal flow pathways in the Cadeby Formation and are characterized by a relatively regular vertical spacing (0.38 m;  $\sigma = 0.57$  m; Tab. 2) in the three boreholes. The number of fractures that localize inflows does not decrease with depth (Tab. 3). Hence, the observed hydraulic conductivity decrease (Fig. 6) cannot be related to vertical variation of fracturing density.

#### 4.4 Hydraulic monitoring

##### 4.4.1 Hydraulic head fluctuation and potential recharge

The hydraulic monitoring realised at the University of Leeds Farm shows a similar pattern of head variation in the three boreholes, with head range of 2.5 – 4.0 m between low in December, 2017 and high in April 2018 (Fig. 7, S2), with almost identical results from loggers installed in piezometers in the same borehole (max difference 5mm), suggesting good hydraulic connectivity between bedding fractures. Temporal changes in hydraulic head are consistent with the potential recharge estimated from the NCAS Weather Station data, i.e a gentle fall in head which reaches the minimum at the end of December 2017 corresponds to a period of negative potential recharge ( $R$ ), see Figures 7A and B. A time lag of three weeks is observed between potential recharge becoming mainly positive in early December and the minimum hydraulic head occurring at the end of that month. Positive potential recharge ( $R$ ) from 26<sup>th</sup> December up to 5<sup>th</sup> April (Fig. 7A), arises from low values of potential evapotranspiration ( $ET_0$ ) occurring during this period. This matches a steep rise in hydraulic head during the winter-spring period which is ~2.5 and ~4 meters in BH2 and BH1/BH3 respectively (Fig. 7B, S2). The hydraulic head reached a maximum in the middle of April (Fig. 7B); the time lag between the switch in potential recharge towards negative values in early April and the peak hydraulic head is ~10 days. Finally, a drop of the water table characterizes the period of late April, May and June when high values of potential evapotranspiration ( $ET_0$ ) exceeds rainfall ( $P$ ) in this period of the hydraulic year (Figs. 7A, B).

#### 4.4.2 Groundwater flow vector

Hourly data of hydraulic gradient and azimuth (found using the averages of hydraulic heads from the piezometers in each borehole, see Figs. 7C, D, 8A, B) show that the hydraulic gradient ranges from 0.0210 to 0.0247 and the arithmetic mean is 0.0236 (Fig. 8A), i.e. relatively minor seasonal variation. The azimuth varies by only  $5.8^\circ$  with a Fisher Mean of  $68.4^\circ$  (Fig. 8B).

The hydraulic gradient is characterized by a very gentle rise during the months of October, November and December (Fig. 7C). This plateau during the autumn produces a cluster of hourly data in the range 0.0240 - 0.0247 (where 45% of hourly data are grouped). The hydraulic gradient drops during the months of January, February, March and early April (Fig. 7C); corresponding with the rise in hydraulic head at the field site. Then, it rises contemporaneously to decreasing hydraulic head in late April, May and June (Figs. 7B, S3).

The direction of the groundwater flow vector is also characterized by minor seasonal variation (Fig. 7D); the azimuth of the vector rotates  $5.8^\circ$  eastwards during the steep rise in hydraulic head during the winter-spring period, and shows a bimodal distribution (Fig. 8B), with 48% and 23% of readings clustered between  $66.5^\circ$ - $67.5^\circ$  and  $71.0^\circ$ - $72.2^\circ$ , respectively. The  $66.5^\circ$ - $67.5^\circ$  cluster is representative of the months of October, November and December; the  $71.0^\circ$ - $72.2^\circ$  cluster is representative of end of April, May and June which are characterized by both a gentle drop of the water table and a little eastward rotation of the groundwater flow vector (Figs. 7B, D). This contrasts the hydrologic scenario of the winter-spring months which are characterized by both a steep rise of the water table ( $\sim 3\text{m}$ ; Fig. 7B) and a sharp eastward rotation of the flow vector (Fig. 7D).

#### 4.5 Hydraulic aperture, fracture flow velocities and regime

Average fracture hydraulic aperture ( $b$ ) at each of the screened intervals is computed using Equation (2);  $b$  ranges from 0.10 up to 0.43 mm (Tab. 4), with smaller values found for increasing depths. Such values are in the range of shallow ( $< \sim 100$  mBGL) fractured aquifers for bedding plane discontinuities and joints ( $\sim 0.01$  - 0.8 mm; Cappa et al., 2008; Quinn et al., 2011; Maldaner et al., 2018; Ren et al., 2018a).

Determination of hydraulic aperture allows computation of the average flow velocity within fractures using Equation (3), based on the measured horizontal hydraulic gradients. Groundwater flow velocities computed using this approach range from 13

up to 242 m/day (Fig. 9). Velocities rapidly decrease with increasing depth in all three boreholes; as a consequence of the depth sensitivity of hydraulic conductivity and hydraulic aperture (see Fig. 6). The first ~ 10 meters below the water table represents the part of the Cadeby Formation which is characterized by relatively high horizontal hydraulic conductivity (Fig. 6;  $K_h = 0.30 - 2.85$  m/day) and flow velocity (Fig. 9;  $V = 33 - 242$  m/day).

Groundwater flow velocities in correspondence of fractures also vary over time, due to variations of hydraulic gradient during the period of the groundwater recharge (Fig. 9, indicated by the horizontal bars). However, this effect is only maximum 15% of the mean value, whereas velocities differs by several times (more than 10 in BH2 and 3) between the upper and lower screened intervals.

The Reynolds ( $Re$ ) number found using Equation (4) varies, in proportion with flow velocities (Fig. 10), from 0.01 up to 1.1. Thus, laminar flow occurs under natural conditions. Notably, the Reynold number in the BH1-P1 screened interval, which is located only ~2m below the water table, partially exceeds the lower limit of the field of laminar/turbulence transition (Fig. 10).

#### 4.6 Insights for contaminant transport

##### 4.6.1 Controls on permeability distribution and flow velocities

Groundwater flow velocities and regime have been determined by applying a cubic law model to the Permian Cadeby Formation of Yorkshire, NE England. Indeed, this is a fracture flow aquifer ( $K_{\text{well-test}}/K_{\text{core-plug}} \sim 10^4$ ) with flow dominated by sub-horizontal ( $< 4^\circ$ ) bedding plane discontinuities with absence of large karstic features ( $>1.5$  mm) as schematically represented in Figure 11.

Inferred hydraulic fracture apertures and hence groundwater flow velocities in this dolostone aquifer of Permian age show strong reduction with increasing depth below the water table. Similar reduction of aperture of discontinuities with depth has been observed in quarries in the Jurassic dolostones of the Venetian Alps in northern Italy and in the Carboniferous limestones of the County Claire in western Ireland (Williams, 1983).

Our findings for the Cadeby Formation of NE Yorkshire are consistent with trends in transmissivity ( $T = 15 - 4300$  m/day;  $n=23$ ) from historical pumping tests in that  $T$  values do not show any correlation with well depths up to ~50 m (Allen et al., 1997), indicating that the permeability with the formation usually resides close to the water

table. Such permeability distributions typically arise from dissolution of calcite and dolomite occurring in the shallowest part of aquifers immediately below the water table, which strongly enhances permeability and fracture apertures (Allen et al., 1997; Göppert, and Goldscheider, 2008; Hartmann et al., 2014). The driving force of carbonate dissolution in carbonate aquifers is represented by elevated  $p\text{CO}_2$  recharge water percolating through the soil zone (Atkinson, 1977; Palner, 1991). This is an active process in the Critical Zone at the University of Leeds Farm site. In fact, research on soil geochemistry at this site has revealed that agriculture activities increase decomposition rates of soil organic matter (SOM). This leads to an increase in the release of carbon dioxide from the soil into the groundwater with consequence  $p\text{CO}_2$  increase (Holden et al., 2019).

As a consequence, the most hazardous part of the Critical Zone for contaminant dispersal in these aquifer types is the uppermost highly permeable ~10 meters below the water table as depicted in the conceptual model in Figure 11. Reynolds number is up to ~1 in this highly permeable upper part of the Critical Zone. Thus, Reynolds number  $> 1$  are likely to occur in more extensively faulted areas where more pervasive flow and carbonate dissolution has occurred. In fact, outcrop observations in areas close to extensional fault traces show cavities 0.1 - 0.7 cm in size in the dolostone of the Cadeby Formation. Single-borehole pumping tests show in this aquifer much higher transmissivities in correspondence of faults ( $T = 790 - 1680 \text{ m}^2/\text{day}$ ;  $n=7$ ) rather than within the unfaulted blocks ( $T = 15 - 210 \text{ m}^2/\text{day}$ ;  $n=16$ ), likely to be a consequence of enhanced carbonate dissolution in association with faults (Allen et al., 1997; Cooper and Lawley, 2007).

At our field site, the hydraulic gradient and hence groundwater velocity does not significantly vary during the hydraulic year (Figs. 7C; 8A; 9). This likely arises from the boundary conditions of the aquifer system at the University of Leeds Farm site, i.e. streams coming from the adjacent hills to the west partially recharge the aquifer, maintaining a stable hydraulic gradient (Aldrick, 1978). These findings indicate how, at least under conditions of relatively minor seasonal hydraulic variation, changes in groundwater flow velocities with depth are much stronger than seasonal fluctuations. In such conditions, steady state groundwater flow models might be adequate to compute solute contaminant transport.

#### 4.6.2 Future research

Future research on fracture-flow carbonate aquifer-types is needed in several directions. We envisage efforts on both characterization of hydraulic conductivity versus depth, and flow and contaminant transport modelling. Hydraulic conductivity can be better constrained in open wells using flow logging (Day-Lewis et al., 2011; Sawdey and Reeve, 2012), FLUTe liner profiling (Quinn et al., 2015; Ren et al., 2018a) and nuclear magnetic resonance (NMR) testing (Walsh et al., 2015; Ren et al., 2018b). All these techniques that have been recently developed for fractured aquifers at shallow depths allow permeability characterization along the entire well (rather than specific intervals).

This research has also shown how the limit of the laminar/turbulent transition field can be reached even in non-faulted blocks of carbonate rocks, in absence of karstic cavities. Thus, flow regime is likely to change as we approach areas of more developed carbonate dissolution, such as extensional faults, which are characterized by high transmissivities, or systems of cavities connected to springs as seen in several carbonate aquifers across the world (Galdenzi and Menichetti, 1995; Raeisi and Karami, 1997; Gallegos et al., 2013; Bauer et al., 2016). Groundwater flow models need to be developed that can be implemented in correspondence of such structures, i.e. to include likely occurrence of turbulence and higher groundwater flow velocities (Hill et al., 2010; Saller et al., 2013).

## 5. Conclusions

Contaminant transport occurs at relatively high velocity in the saturated parts of shallow fractured aquifers, and this may be very important in areas of arable and livestock farming activity. Here, we report an investigation of the Critical Zone of a fractured dolostone aquifer (Permian dolostone of the Cadeby Formation) beneath the University of Leeds Farm, Yorkshire. A combination of fluid logging, slug tests and hydraulic head monitoring was used. Outputs from these techniques were applied to a parallel plate model to determine the spectrum of flow velocities and establish occurrence of laminar or turbulent flow.

Fluid temperature and conductivity logs identified the bedding plane fractures as principal flow pathways which is a common hydraulic feature in fractured carbonate aquifers. Hydraulic testing (e.g., slug tests) allows determination of the hydraulic fracture aperture by applying the cubic law. Determination of hydraulic gradient from hydraulic head monitoring then allows the determination of the spectrum of

groundwater velocities in time and space. Indeed, this workflow was applied at shallow ( $< \sim 40$  mBGL) depths in a non-faulted part of the Permian dolostone of the Cadeby Formation. It produced fracture flow velocities ranging from 13 up to 242 m/day. Depth variations of fracture flow velocities are found much more significant than seasonal variations.

The upper  $\sim 10$  meters immediately below the water table were most highly hydraulically conductive ( $K_h = 0.30 - 2.85$  m/day) and characterized by elevated groundwater flow velocities ( $V = 33 - 242$  m/day) due to the processes of fracture aperture enhancement by carbonate dissolution which are typical of fractured carbonates. Hence, these  $\sim 10$  meters represent the most hazardous part of the Critical Zone for contaminant transport. As a consequence, we envisage further efforts on characterization of permeability with depth in the Critical Zone of fractured carbonate aquifers.

Another key finding is that within unfaulted blocks in absence of large karstic cavities the Reynolds number may reach  $\sim 1$ . Thus, turbulent flow is likely to arise as we approach tectonic structures (e.g., normal faults) which are characterized by enhanced carbonate dissolution and macro-karstic features. Groundwater flow models must be developed that represent flow as turbulent in correspondence of such tectonic structures.

### **Acknowledgements**

The authors thank NERC (CZO: Using Critical Zone Science-Peri Urban Agriculture in China Grant) for funding this research project. Drilling and well logging were conducted in July 2017 by European Geophysical Services Ltd and ESG, respectively. Measurement of well top position and elevation has been carried out by Subsans UDS in April 2018. Edward Wrathmell and Harris Tarnanas (both Environment Agency) gave useful advices at the beginning of the project. Technical advice on the organization of the NCAS Station hydrologic dataset were kindly provided by David Boorman (Centre for Ecology & Hydrology, Wallingford). Graduate students Claire Boddy and Stephen Gillham are thanked for performing discontinuity surveys and slug tests at the field site.

The results of this research also benefitted from discussions with John Walsh (University College Dublin), Noelle Odling (former University of Leeds), Carlos Grattoni (University of Leeds), Pippa Chapman (University of Leeds) and Susan

Wagstaff (JBA Consulting) regarding the geological heterogeneities and the hydrogeology of fractured carbonate aquifers. Finally, we thank George Sorensen, University of Leeds Farm Manager, for his assistance in arranging instrumentation installation and logistics.

## References

- Abesser C, Lewis M., 2015. A semi-quantitative technique for mapping potential aquifer productivity on the national scale: example of England and Wales (UK). *Hydrogeol. J.* 23(8), 1677-1694.
- Aitkenhead, N., 2002 *The Pennines and Adjacent areas*. British Geological Survey, Nottingham, England (UK).
- Aldrick, R.J., 1978. The hydrogeology of the Magnesian Limestones in Yorkshire between the River Wharfe and the River Aire. *Quart. J. Engineer. Geol. Hydrogeol.* 11 (2), 193-201.
- Allen D.J., Brewerton L.M., Coleby B.R., Gibbs M.A., Lewis A., MacDonald SJ, Wagstaff, A.T., Williams L.J., 1997. *The Physical Properties of Major Aquifers in England and Wales*. Technical Report WD/97/34, 157-287. British Geological Survey, Nottingham, England (UK).
- Allimendinger R.W., Cardozo N., Fisher D., 2012. *Structural Geology Algorithms: Vectors and Tensors*. Cambridge University Press, Cambridge, England (UK).
- Anderson, S.P., Bales, R.C., Duffy, C.J., 2008. Critical Zone Observatories: Building a network to advance interdisciplinary study of Earth surface processes. *Mineral. Mag.*, 72(1), 7-10.
- Atkinson, T.C., 1977. Carbon dioxide in the atmosphere of the unsaturated zone: an important control of groundwater hardness in limestones. *J. Hydrol.* 35(1-2), 111-123.
- Bailly-Comte, V., Martin, J.B., Jourde, H., Sreaton, E.J., Pistre, S., Langston, A., 2010. Water exchange and pressure transfer between conduits and matrix and their influence on hydrodynamics of two karst aquifers with sinking streams. *J. Hydrol.* 386, 55-66.

Banwart, S, Bernasconi S.M., Bloem J., Blum W., Brandao M., Brantley S., Chabaux F., Duffy, C., Kram, P., Lair, G., Lundin, L., 2011. Soil processes and functions in critical zone observatories: hypotheses and experimental design. *Vadose Zone J.* 10(3), 974-87.

Banwart, S., Menon, M., Bernasconi, S.M., Bloem, J., Blum, W.E., de Souza, D.M., Davidsdotir, B., Duffy, C., Lair, G.J., Kram, P., Lamacova, A., 2012. Soil processes and functions across an international network of Critical Zone Observatories: Introduction to experimental methods and initial results. *Comptes Rendus Geosci.*, 344(11-12), 758-772.

Bauer H, Schröckenfuchs TC, Decker K., 2016. Hydrogeological properties of fault zones in a karstified carbonate aquifer (Northern Calcareous Alps, Austria). *Hydrogeol. J.* 24. 1147–1170.

Beljin, M., Ross, R.R., Acree, S.D., 2014. 3PE: A Tool for Estimating Groundwater Flow Vectors. Report EPA 600/R-14/273. United States Environmental Protection Agency, Ada, Oklahoma (USA).

Berkowitz, B. 2002. Characterizing flow and transport in fractured geological media: A review. *Advan. Water Resour.* 25, 861-884.

Berkowitz, B., Bear, J., Braester, C., 1988. Continuum models for contaminant transport in fractured porous formations. *Water Resour. Resear.* 24(8), 1225-1236.

Blatt, H., Middleton, G.V., Raymond, C., 1972. Murray. Origin of sedimentary rocks. (1972). AbeBooks, Victoria (Canada)

Bloomfield J.P., Williams R.J., Goody D.C., Cape J.N., Guha, P.M., 2006. Impacts of climate change on the fate and behaviour of pesticides in surface and groundwater—a UK perspective. *Sci. Total Environ.* 369, 163-177.

Boddy, C., 2018. Hydraulic characterization of the Cadeby Formation in the Tadcaster area (Yorkshire, NE England. MSc Thesis, University of Leeds (UK).

Bottrell S.H., West L.J., Yoshida K., 2006. Combined isotopic and modelling approach to determine the source of saline groundwaters in the Selby Triassic sandstone aquifer, UK. In: Barker, R.D., Tellam, J.H. (Eds.), *Fluid Flow and Solute Movement in Sandstones: The Onshore UK Permo-Triassic Red Bed Sequence.* Geol. Soc. London, Spec. Publ., 263, pp.325-338.

- Bouwer H., Rice R.C., 1976. A slug test for determining hydraulic conductivity of unconfined aquifers with completely or partially penetrating wells. *Water Resour. Res.* 12 (3), 423-428.
- Bricker S.H., Barkwith A.K.A.P., MacDonald A.M., Hughes A.G., Smith M., 2012. Effects of CO<sub>2</sub> injection on shallow groundwater resources: A hypothetical case study in the Sherwood Sandstone aquifer, UK. *Int. J. Greenhouse Gas Control.* 11, 337-348.
- Butler, J.J., 1998. The design, performance, and analysis of slug tests. Lewis, Boca Raton, Florida (USA).
- Cai, Z., Merly, C., Thomson, N. R., Wilson, R. D., Lerner, D. N. 2007. Channel flow and trichloroethylene treatment in a partly iron-filled fracture: Experimental and model results. *J. Contam. Hydrol.* 93(1-4), 284-303.
- Cairney, T., 1972. Hydrological investigation of the Magnesian Limestone of south-east Durham, England. *J. Hydrol.* 16 (4), 323-340.
- Canter, L. W., 1996. Nitrates in groundwater. CRC press, Boca Raton (Florida, USA).
- Cappa, F., Guglielmi, Y., Rutqvist, J., Tsang, C.F., Thoraval, A., 2008. Estimation of fracture flow parameters through numerical analysis of hydromechanical pressure pulses. *Water Resour. Resear.* 44(11).
- Cheong, J.Y., Hamm, S.Y., Kim, H.S., Ko, E.J., Yang, K., Lee, J.H., 2008. Estimating hydraulic conductivity using grain-size analyses, aquifer tests, and numerical modeling in a riverside alluvial system in South Korea. *Hydrogeol. J.*, 16(6), 1129.
- Christensen, T.H., Bjerg, P. L., Banwart, S. A., Jakobsen, R., Heron, G., Albrechtsen, H. J., 2000. Characterization of redox conditions in groundwater contaminant plumes. *J. Contam. Hydrol.* 45(3-4), 165-241.
- Conboy, M.J., Goss, M.J., 2000. Natural protection of groundwater against bacteria of fecal origin. *J. Contam. Hydrol.* 43(1), 1-24.
- Cooper A.H., Lawley R.S., 2007. Tadcaster Magnesian Limestone 3-D borehole interpretation and cross-sections study. British Geological Survey, Nottingham, England (UK).

- Danielopol, D.L., Griebler, C., Gunatilaka, A., Notenboom, J., 2003. Present state and future prospects for groundwater ecosystems. *Environ. Conserv.* 30, 2, 104-130.
- Day-Lewis, F.D., Carole, D.J., Frederick, L.P., Keith, J.H., 2011. A computer program for flow-log analysis of single holes (FLASH). *Groundwater* 49, 6, 926-931.
- Dogliani, C., 1994. Foredeeps versus subduction zones. *Geology* 22(3), 271-274.
- Farrant A.R., Cooper A.H., 2008. Karst geohazards in the UK: the use of digital data for hazard management. *Quart. J. Engineer. Geol. Hydrogeol.* 41(3), 339-356.
- Ford, D.C., Williams, P.W., 1989. Karst geomorphology and hydrology. Unwin Hyman, London (UK).
- Foster S.S.D., 1976. The vulnerability of British groundwater resources to pollution by agriculture leachates. *M.A.F.F. Tech Bull.* 32, 159-165.
- Foster S.S.D., Crease R.I., 1974. Nitrate pollution of Chalk groundwater in East Yorkshire – a hydrogeological appraisal. *J. Inst. Wat. Engrs.* 28, 178-194.
- Forster S.S.D., Cripps A.C., Smith-Carington A., 1982. Nitrate leaching to groundwater. *Phil. Trans. R. Soc. Lond.* 296, 477-489.
- Fouillac, A.M., Muller, D., Negrel, P., Darmendrail, D., Slob, A.F., Grath, J., Scheidleder, A., Rodgers-Jenkins, C., Galbiati, L., Bidoglio, G., Arnold, G., 2007. Groundwater science and policy: an international overview. Royal Society of Chemistry, Cambridge (UK).
- Galdenzi, S., Menichetti, M., 1995. Occurrence of hypogenic caves in a karst region: examples from central Italy. *Environment. Geol.* 26(1), 39-47.
- Gallegos, J.J., Hu, B.X., Davis, H., 2013. Simulating flow in karst aquifers at laboratory and sub-regional scales using MODFLOW-CFP. *Hydrogeol. J.* 21(8), 1749-1760.
- Gaunt, G.D., Coope, G.R., Franks, J.W., 1970. Quaternary deposits at Oxbow opencast coal site in the Aire Valley, Yorkshire. *Proceed. York. Geol. Soc.* 38(2), 175-200.
- Gellasch C.A., Bradbury K.R., Hart D.J., Bahr J.M., 2013. Characterization of fracture connectivity in a siliciclastic bedrock aquifer near a public supply well (Wisconsin, USA). *Hydrogeol. J.* 21 (2), 383-399.

- Göppert, N., Goldscheider, N. 2008. Solute and colloid transport in karst conduits under low-and high-flow conditions. *Groundwater* 46, 61-68.
- Guy, K.A., Xu, H., Yang, J.C., Werth, C.J., Shapley, J.R. 2009. Catalytic nitrate and nitrite reduction with Pd- Cu/PVP colloids in water: Composition, structure, and reactivity correlations. *J. Phys. Chem.* 113(19), 8177-8185.
- Guzzetta G., 1984. Kinematics of stylolite formation and physics of the pressure-resolution process. *Tectonophysics* 101, (3-4), 383-394.
- Hartmann, A., Goldscheider, N., Wagener, T., Lange, J. Weiler, M., 2014. Karst water resources in a changing world: Review of hydrological modeling approaches. *Reviews Geophys.* 52(3), 218-242.
- Hartmann S., Odling N.E., West L.J., 2007. A multi-directional tracer test in the fractured Chalk aquifer of E. Yorkshire, UK. *J. Contam. Hydrol.* 94 (3), 315-331.
- Hyder Z., Butler J.J., 1995. Slug tests in unconfined formations: An assessment of the Bouwer and Rice technique. *Groundwater* 33 (1), 16-22.
- Hill, M.E., Stewart, M.T., Martin, A., 2010. Evaluation of the MODFLOW-2005 conduit flow process. *Groundwater* 48, 4, 549-559.
- Hitchmough A.M., Riley M.S., Herbert A.W., Tellam J.H., 2007. Estimating the hydraulic properties of the fracture network in a sandstone aquifer. *J. Contam. Hydrol.* 93 (1), 38-57.
- Holden, J., Grayson, R., Berdeni, D., Bird, S., Chapman, P.J., Edmondson, J.L., Firbank, L.G., Helgason, T., Hodson, M.E., Hunt, S., Jones, D.T., Lappage, M., Marshall-Harries, E., Nelson, M., Prendergast-Miller, M., Shaw, H., Wade, R., Leake, J.R., 2018. The role of hedgerows in soil functioning within agricultural landscapes. *Agr. Ecosyst. Environ.* 273, 1-12.
- Ji, S.H., Koh, Y.K., 2015. Nonlinear groundwater flow during a slug test in fractured rock. *J. Hydrol.* 520, 30-36.
- Ji S.H., Lee H.B., Yeo I.W., Lee K.K., 2008. Effect of nonlinear flow on DNAPL migration in rough-walled fracture. *Water. Resour. Res.* 44, W11431.
- Jourde, H., Cornaton, F., Pistre, S., Bidaux, P., 2002. Flow behavior in a dual fracture network. *J. Hydrol.* 266, 1-2, 99-119.

- KGS, 1985. The Kansas Geological Survey Model for slug tests. Environmental Simulations International, Shrewsbury (UK)
- Kortas L., Younger P.L., 2013. Fracture patterns in the Permian Magnesian Limestone Aquifer, Co. Durham, UK. *Proceed. York. Geol. Soc.* 59(3), 161-171.
- Lee, M.R., 1993. Formation and diagenesis of slope limestones within the Upper Permian (Zechstein) Raisby Formation, north-east England. *Proceed. York. Geol. Polytech. Soc.* 9 (3), 215-227.
- Lott, G.K., Cooper, A.H., 2005. The building limestones of the Upper Permian, Cadeby Formation (Magnesian Limestone) of Yorkshire. Report IR/05/048, British Geological Survey, Nottingham (UK)
- Lerner D.N., Harris B., 2009. The relationship between land use and groundwater resources and quality. *Land Use Pol.* 26, 2009, 265-273.
- Lo H.C., Chen P.J., Chou P.Y., Hsu, S.M., 2014. The combined use of heat-pulse flowmeter logging and packer testing for transmissive fracture recognition. *J. Applied Geophys.* 105, 48-258.
- Lott, G.K., Richardson, C., 1997. Yorkshire stone for building the Houses of Parliament (1839–c. 1852). *Proceed. York. Geol. Polytech. Soc.* 51 (4), 265-272.
- Lott G., 2013. Sourcing stone for the conservation and repair of historical buildings in Britain. *Q. J. Engineer. Geol. Hydrogeol.* 46(4), 405-420.
- Maldaner, C.H., Quinn, P.M., Cherry, J.A., Parker, B.L., 2018. Improving estimates of groundwater velocity in a fractured rock borehole using hydraulic and tracer dilution methods. *J. Contam. Hydrol.* 214, 75-86.
- Mayes, W.M., Large, A.R.G., Younger, P.L., 2005. The impact of pumped water from a de-watered Magnesian limestone quarry on an adjacent wetland: Thrislington, County Durham, UK. *Environ. Pollut.* 138, 3, 443-454.
- McKay L.D., Cherry J.A., Gillham R.W., 1993. Field experiments in a fractured clay till: 1. Hydraulic conductivity and fracture aperture. *Water Resour. Resear.* 29, 1149-1162.

- Meckenstock, R.U., Morasch B., Griebler C., Richnow H.H., 2004. Stable isotope fractionation analysis as a tool to monitor biodegradation in contaminated aquifers. *J. Contam. Hydrol.* 75, 215-255.
- Medici G., Boulesteix K., Mountney N.P., West L., Odling N.E., 2015. Palaeoenvironment of braided fluvial systems in different tectonic realms of the Triassic Sherwood Sandstone Group, UK. *Sediment. Geol.* 329, 188-210.
- Medici G., West L.J., Mountney N.P., 2016. Characterizing flow pathways in a sandstone aquifer: Tectonic vs sedimentary heterogeneities. *J. Contam. Hydrol.* 194, 36-58.
- Medici G., West L.J., Mountney N.P., 2018a. Characterization of a fluvial aquifer at a range of depths and scales: the Triassic St Bees Sandstone Formation, Cumbria, UK. *Hydrogeol. J.* 26(2), 565-591.
- Medici G., West L.J., Mountney N.P., 2018b. Sedimentary flow heterogeneities in the Triassic UK Sherwood Sandstone aquifer: Insights for hydrocarbon exploration. *Geol. J.* <https://doi.org/10.1002/gj.3233>
- Mellor, A.F.P, Cey, E.E., 2015. Using generalized additive mixed models to assess spatial, temporal, and hydrologic controls on bacteria and nitrate in a vulnerable agricultural aquifer. *J. Contam. Hydrol.* 182, 104-116.
- Mondal, P.K., Sleep, B.E., 2012. Colloid transport in dolomite rock fractures: Effects of fracture characteristics, specific discharge, and ionic strength. *Environ. Sci. Technol.* 46(18), 9987-9994.
- Mondal, P.K., Sleep, B.E., 2013. Virus and virus-sized microsphere transport in a dolomite rock fracture. *Water Resour. Resear.* 49(2), 808-824.
- Neymeyer A.R.T., Williams P.L., Younger P.L., 2007. Migration of polluted mine water in a public supply aquifer. *Quart. J. Engineer. Geol. Hydrogeol.* 40, (1)75-84.
- Odling N.E., Gillespie P., Bourguine B., Castaing C., Chiles J.P., Christensen N.P., Fillion E., Genter A., Olsen C., Thrane L., Trice R., 1999. Variations in fracture system geometry and their implications for fluid flow in fractured hydrocarbon reservoirs. *Petrol Geosci.* 1999 5(4), 373-84.

- Odling N.E., Roden J.E., 1997. Contaminant transport in fractured rocks with significant matrix permeability, using natural fracture geometries. *J. Contam. Hydrol.* 27(3-4), 263-283.
- Odling N.E., West L.J., Hartmann S., Kilpatrick A., 2013. Fractional flow in fractured chalk; a flow and tracer test revisited. *J. Contam. Hydrol.* 147, 96-111.
- Park W.C., Schot E.H., 1968. Stylolites: their nature and origin. *Journal of Sedimentary Research*, 38(1). DOI 10.1306/2F74D71910-2B21-1
- Peryt T.M., Scholle, P.A., 1996. Regional setting and role of meteoric water in dolomite formation and diagenesis in an evaporite basin: studies in the Zechstein (Permian) deposits of Poland. *Sedimentology*, 43(6), 1005-1023.
- Petitta M., Fracchiolla D., Aravena R., Barbieri M., 2009. Application of isotopic and geochemical tools for the evaluation of nitrogen cycling in an agricultural basin, the Fucino Plain, Central Italy. *J. Hydrol.* 372, 124-135.
- Palmer, A.N. 1991. Origin and morphology of limestone caves. *Geol. Soc. America Bulletin.*, 103(1), 1-21.
- Qian J., Chen Z., Zhan H., Guan H., 2011. Experimental study of the effect of roughness and Reynolds number on fluid flow in rough-walled single fractures: a check of local cubic law. *Hydrol. Proces.* 25(4), 614-622.
- Quinn, P., Cherry, J.A., Parker, B.L., 2015. Combined use of straddle packer testing and FLUTE profiling for hydraulic testing in fractured rock boreholes. *J. Hydrol.* 524, 439-454.
- Quinn, P.M., Parker B.L., Cherry J.A., 2011. Using constant head step tests to determine hydraulic apertures in fractured rock. *J. Contam. Hydrol.* 126(1), 85-99.
- Raeisi, E., Karami, G., 1997. Hydrochemographs of Berghan karst spring as indicators of aquifer characteristics. *J. Caves Karst Stud.*, 59(3), 112-118.
- Ranjith, P.G., Darlington, W., 2007. Nonlinear single-phase flow in real rock joints. *Water Resour. Res.* 43, W09502.
- Re V., Sacchi E, Kammoun S, Tringali C, Trabelsi R, Zouari K, Daniele S., 2017. Integrated socio-hydrogeological approach to tackle nitrate contamination in

groundwater resources. The case of Grombalia Basin (Tunisia). *Sci. Total Environ.* 593, 664-676.

Ren S., Gragg S., Zhang Y., Carr B., Yap, G., 2018a. Borehole characterization of hydraulic properties and groundwater flow in a crystalline fractured aquifer of a headwater mountain watershed, Laramie Range, Wyoming. *J. Hydrol.* 561, 780-795.

Ren, S., Parsekian, A.D., Zhang, Y., Bradley J.C., 2018b. Hydraulic conductivity calibration of logging NMR in a granite aquifer, Laramie Range, Wyoming. *Groundwater*, *in press*.

Rivett, M.O., Smith, S.R., Buss, M., 2007. Nitrate occurrence and attenuation in the major aquifers of England and Wales. *Quart. J. Engineer. Geol. Hydrogeol.* 40(4), 335-352.

Rivett M.O., Buss S.R., Morgan P., Smith J.W., Bemment C.D., 2008 Nitrate attenuation in groundwater: a review of biogeochemical controlling processes. *Water Resear.* 42(16), 4215-4232.

Romm, E. S., 1966. *Flow Characteristics of Fractured Rocks* (in Russian). Nedra, Moscow (Russia).

Saller, S.P., Ronayne, M.J., Long, A.J., 2013. Comparison of a karst groundwater model with and without discrete conduit flow. *Hydrogeol. J.* 21, 7, 1555-1566.

Sawdey, J.R., Reeve, A.S., 2012. Automated inverse computer modeling of borehole flow data in heterogeneous aquifers. *Comput. Geosci*, 46, 219-228.

Skaggs, T.H., Kabala, Z.J., 1998. Limitations in recovering the history of a groundwater contaminant plume. *J. Contam. Hydrol.* 33(3-4), 347-359.

Smith D.B., Harwood G.M., Pattison J., Pettigrew T.H., 1986. A revised nomenclature for Upper Permian strata in eastern England, in: Harwood, G.M., Smith D.B. (Eds.), *The English Zechstein and Related Topics*. *Geol. Soc. London Spec. Publ.*, 22(1), pp.9-17.

Stein, H., Kellermann, C., Schmidt, S. I., Brielmann, H., Steube, C., Berkhoff, S. E., Griebler, C., 2010. The potential use of fauna and bacteria as ecological indicators for the assessment of groundwater quality. *J. Environment. Monitor.* 12(1), 242-254.

- Tallini, M., Parisse, B., Petitta, M., Spizzico, M., 2013. Long-term spatio-temporal hydrochemical and  $^{222}\text{Rn}$  tracing to investigate groundwater flow and water–rock interaction in the Gran Sasso (central Italy) carbonate aquifer. *Hydrogeol. J.* 21(7), 1447-1467.
- Tellam, J.H., Barker R.D., 2006. Towards prediction of saturated-zone pollutant movement in groundwaters in fractured permeable-matrix aquifers: the case of the UK Permo-Triassic sandstones, in: Barker, R.D., Tellam, J.H. (Eds.), *Fluid Flow and Solute Movement in Sandstones: The Onshore UK Permo-Triassic Red Bed Sequence*. Geol. Soc. London, Spec. Publ. 263, pp.1-48.
- Terzaghi, R.D., 1965. Sources of errors in joint surveys. *Geotechnique*, 15 (3), 287-304.
- Thorbjarnarson, K.W., Mackay, D.M., 1997. A field test of tracer transport and organic contaminant elution in a stratified aquifer at the Rocky Mountain Arsenal (Denver, Colorado, USA). *J. Contam. Hydrol.* 24(3-4), 287-312.
- Thornton, S.F., Lerner, D.N., Banwart, S.A., 2001. Assessing the natural attenuation of organic contaminants in aquifers using plume-scale electron and carbon balances: model development with analysis of uncertainty and parameter sensitivity. *J. Contam. Hydrol.* 53, 199-232.
- Tsang, C.F., Hufschmied, P., Hale, F.V., 1990. Determination of fracture inflow parameters with a borehole fluid conductivity logging method. *Water Resour. Resear.* 26, 4, 561-578.
- Tucker, M.E., 1991. Sequence stratigraphy of carbonate-evaporite basins: models and application to the Upper Permian (Zechstein) of northeast England and adjoining North Sea. *J. Geol. Soc.* 148(6), 1019-1036.
- Wakida, F.T., Lerner, D.N., 2005. Non-agricultural sources of groundwater nitrate: a review and case study. *Water Resear.* 39(1), 3-16.
- Walker, C.D., 2006. A physical and hydrochemical investigation of the Magnesian Limestone in the Tadcaster area, North Yorkshire. MSc Thesis, University of Leeds (UK).
- Walker T.R., 1967. Formation of red beds in modern and ancient deserts. *Geol. Soc. Am. Bull.* 78, 353-368

- West, L.J., Truss, S.W., 2006. Borehole time domain reflectometry in layered sandstone: Impact of measurement technique on vadose zone process identification. *J. Hydrol.* 319 (1), 143-162.
- Williams, J.H., Johnson, C.D., 2004. Acoustic and optical borehole-wall imaging for fractured-rock aquifer studies. *J. Appl. Geophys.* 55(1), 151-159.
- Williams, P.W., 1983. The role of the subcutaneous zone in karst hydrology. *J. Hydrol.* 61(1-3), 45-67.
- Winter, C.L., Tartakovsky, D.M., Guadagnini, A., 2003. Moment differential equations for flow in highly heterogeneous porous media. *Surv. Geophys.* 24(1), 81-106.
- Witherspoon, P.A., Wang, J.S.Y., Iwai, K., Gale, J.E., 1980. Validity of cubic law for fluid flow in a deformable rock fracture. *Water Resour. Resear.* 16, 6, 1016-1024.
- Younger, P.L., 1995. Hydrogeochemistry of minewaters flowing from abandoned coal workings in County Durham. *Quart. J. Engineer. Geol. Hydrogeol.*, 28(2), 101-113.
- Zhang, R., Shuai, D., Guy, K.A., Shapley, J.R., Strathmann, T. J., Werth, C.J., 2013. Elucidation of nitrate reduction mechanisms on a Pd-In bimetallic catalyst using isotope labeled nitrogen species. *Chem. Cat. Chem.*, 5(1), 313-321.
- Zimmerman, R.W., Al-Yaarubi, A., Pain, C.C., Grattoni, C.A., 2004. Non-linear regimes of fluid flow in rock fractures. *Internat. J. Rock Mechan. Mining Sci.*, 41, 163-169.

### Table captions

**Table 1.** Construction details for the three logged boreholes.

**Table 2.** Vertical spacing data for fractures detected by logging in the three boreholes.

**Table 3.** Fractures detected by the optical and acoustic televiewer logs vs. flowing fractures picked using fluid and temperature fluid logs within each screen interval.

**Table 4** Construction details, transmissivity, number flowing fractures and computed values of average hydraulic apertures for each screened interval.

**Table S1.** Horizontal hydraulic conductivity ( $K_h$ ) from slug test analysis: Bouwer and Rice (1976) vs. KGS (1985) models.

### Figure captions

**Fig. 1** Study area. (A) Map depicting location of the study area (basemap from GeoMapApp), (B) geological map and stratigraphic column of the study area, (C) geological cross section based on the interpretation of the Tadcaster EW S2 seismic line, (D) map showing geology, location and elevation of the three drilled boreholes and the NCAS weather station at the field site.

**Fig. 2** Outcrop expression of the Cadeby Formation at Highmoor Quarry (see location in Fig. 1D). (A) Photograph and panel showing bedding plane fractures (Bp), non-stratabound joints (J) and (b) stylolites (St), (B) detail of stylolites (St).

**Fig. 3** Section from optical, and acoustic televiewer logs. (A) Vertical joints (D4) in BH2 borehole, (B) bedding plane fracture (D1) in BH2 borehole, (C) stylolites (D2) in BH2 borehole, (D) cluster of bedding plane fractures (D1) in BH3 borehole.

**Fig. 4** Stereoplots (upper hemisphere, equal area) for all the three wells; (A) Pole diagrams and Kamb Contours of rock discontinuities, (B) Mean vector statistics for the four families of discontinuities with indication of dip direction (Di), dip angle (Da) and magnitude of mean vectors (MV).

**Fig. 5** Fluid temperature and electric conductivity logs with indication of screened intervals (S) and inflows in and out of screened intervals (BH3).

**Fig. 6** Average horizontal hydraulic conductivity from the KGS (1985) analysis of slug tests undertaken in BH1, BH2 and BH3; vertical bar indicates the screen length.

**Fig. 7** Hydrology at the University of Leeds Farm site. (A) Potential groundwater recharge (NCAS Weather Station data), (B) variation of hydraulic head, BH3, (C) hydraulic gradient vs. time, (D) azimuth groundwater flow vector vs time.

**Fig. 8** Frequency histograms from the monitoring of the water table from 1<sup>st</sup> October 2017 to 31<sup>st</sup> June 2018. (A) Hydraulic gradient, (B) azimuth flow directions.

**Fig. 9** Arithmetic mean (square), range of groundwater flow velocity (horizontal bar) at the height screened intervals (vertical bar) and range of fluctuation of the water table (triangles).

**Fig. 10** Arithmetic mean (dot) and range (horizontal bar) of Reynolds Number at the depths of each screened interval (indicated by vertical bar)

**Fig. 11** Conceptual model of fluid flow on a fractured carbonate aquifer at shallow (< ~40 mBGL) depths.

### Supplementary material captions

**Fig. S1** Fluid temperature and electric conductivity logs with indication of screened intervals (S) and inflows in and out of screened intervals; (A) BH1, (B) BH2.

**Fig. S2** Hydraulic head fluctuations at the University of Leeds Farm, (A) BH1, (B) BH2.

ACCEPTED MANUSCRIPT

| Borehole code | Latitude; Longitude         | Borehole diameter (m) | Casing Top (mASL) | Zone | Screened interval depth (BGL; ASL) |
|---------------|-----------------------------|-----------------------|-------------------|------|------------------------------------|
| BH1           | 53°51'54.07"N; 1°18'40.27"W | 0.28                  | 44.71             | P1   | 24.0-27.0; 20.7-17.7               |
|               |                             |                       |                   | P2   | 30.7-33.0; 15.0-11.7               |
| BH2           | 53°51'48.83"N; 1°19'14.18"W | 0.23                  | 46.92             | P1   | 12.2-15.3; 34.9-31.1               |
|               |                             |                       |                   | P2   | 17.0-20.0; 29.9-26.9               |
|               |                             |                       |                   | P3   | 22.5-26.5; 25.4-21.4               |
| BH3           | 53°52'08.32"N; 1°19'10.31"W | 0.28                  | 54.92             | P1   | 25.6-28.6; 25.3-22.3               |
|               |                             |                       |                   | P2   | 31.7-34.0; 19.2-16.9               |
|               |                             |                       |                   | P3   | 37.0-40.0; 13.9-10.9               |

Tab.1

| Fractures               | Code | Population (n.) | Vertical spacing range (m) | Average vertical spacing (m) | Standard deviation $\sigma$ (m) |
|-------------------------|------|-----------------|----------------------------|------------------------------|---------------------------------|
| Bedding plane fractures | D1   | 192             | 0.01-4.10                  | 0.38                         | 0.57                            |
| Stylolites              | D2   | 55              | 0.10-4.50                  | 1.16                         | 2.00                            |
| Joint                   | D3   | 9               | 0.25-20.31                 | 7.04                         | 9.38                            |
| Joint                   | D4   | 8               | 1.44-19.25                 | 8.49                         | 7.72                            |

**Tab. 2**

| Depth screened interval (mBGL) | Number of fractures from borehole televiewer (D1, D3, D4) | Number of flowing fractures |
|--------------------------------|---|-----------------------------|
| <b>Borehole BH1</b>            |   |                             |
| 24.0-27.0                      | 7   | 2                           |
| 30.7-33.0                      | 7   | 3                           |
| <b>Borehole BH2</b>            |   |                             |
| 12.1-15.5                      | 10  | 3                           |
| 17.0-20.0                      | 6   | 3                           |
| 22.0-26.0                      | 6   | 5                           |
| <b>Borehole BH3</b>            |   |                             |
| 25.6-28.6                      | 5   | 5                           |
| 31.7-34.0                      | 3   | 3                           |
| 37.0-40.0                      | 5   | 5                           |

Tab. 3

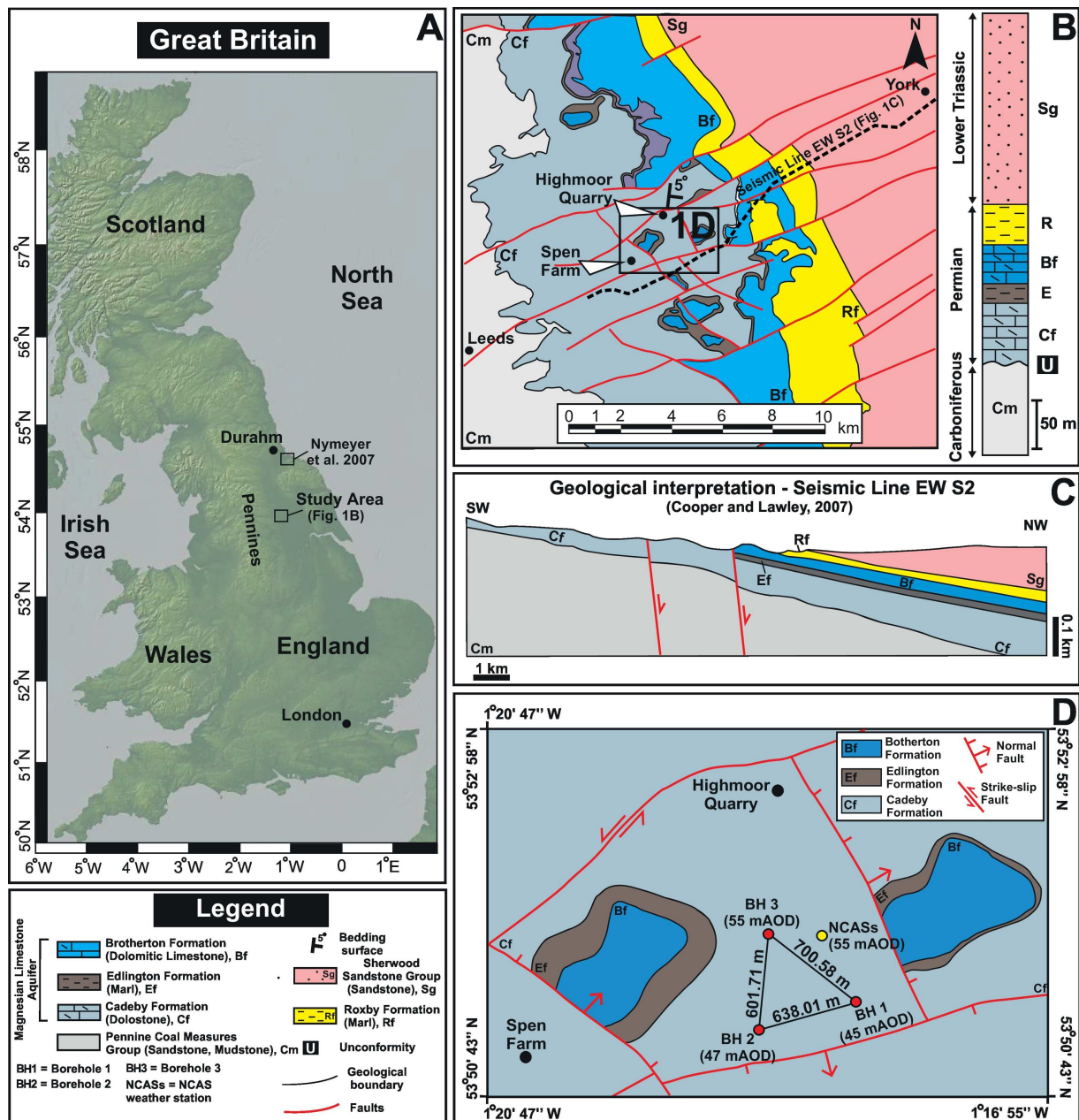
| Screened interval | Screened interval thickness, w (m) | Number of fractures, televiewer logging (D1, D3, D4) | Number of flowing fractures, n | Average Transmissivity, $T_s$ ( $m^2/day$ ) | Average hydraulic aperture, b (mm) |
|-------------------|------------------------------------|--|--------------------------------|---|------------------------------------|
| BH01 P1           | 3.0                                | 2  | 2                              | 8.55  | 0.43                               |
| BH01 P2           | 2.3                                | 3  | 3                              | 5.76  | 0.33                               |
| BH02 P1           | 3.0                                | 3  | 3                              | 5.74  | 0.33                               |
| BH02 P2           | 3.0                                | 3  | 3                              | 2.49  | 0.25                               |
| BH02 P3           | 3.0                                | 5  | 5                              | 0.36  | 0.11                               |
| BH03 P1           | 3.0                                | 5  | 5                              | 0.89  | 0.16                               |
| BH03 P2           | 2.3                                | 3  | 2                              | 0.44  | 0.16                               |
| BH03 P3           | 3.0                                | 5  | 5                              | 0.22  | 0.10                               |

Tab. 4

### Highlights

- Groundwater flow velocity in a shallow ( $\leq 40$  mBGL) fractured carbonate aquifer
- Groundwater flow velocities rapidly decrease with depth in the Critical Zone
- The upper  $\sim 10$  metres below the water table are highly hydraulically conductive
- Laminar flow characterizes the aquifer in un-faulted sections
- Turbulent flow likely arises in correspondence of extensional faults

ACCEPTED MANUSCRIPT



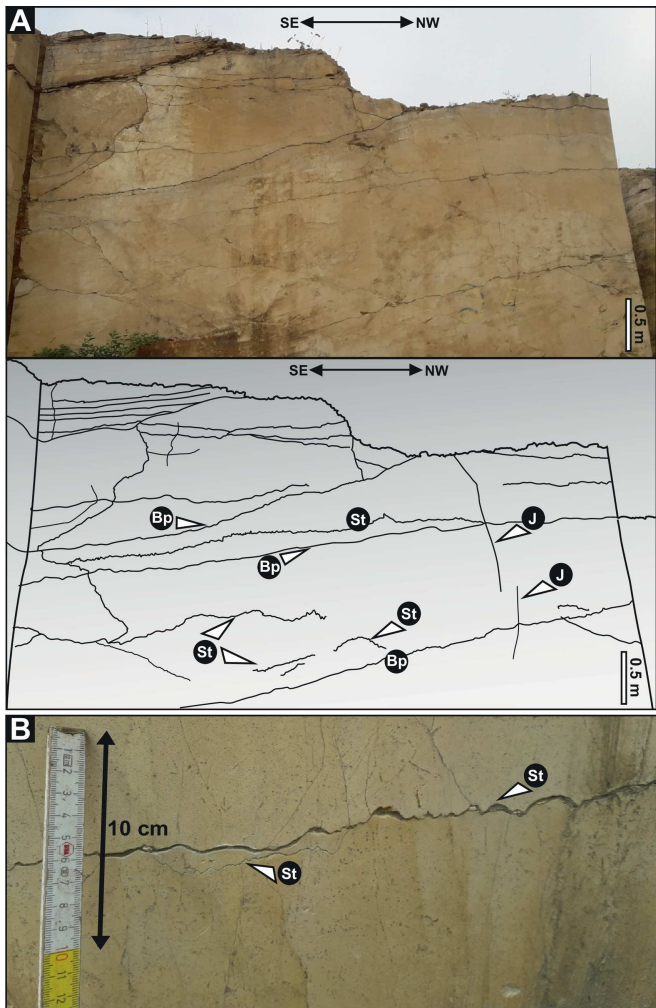


Figure 2

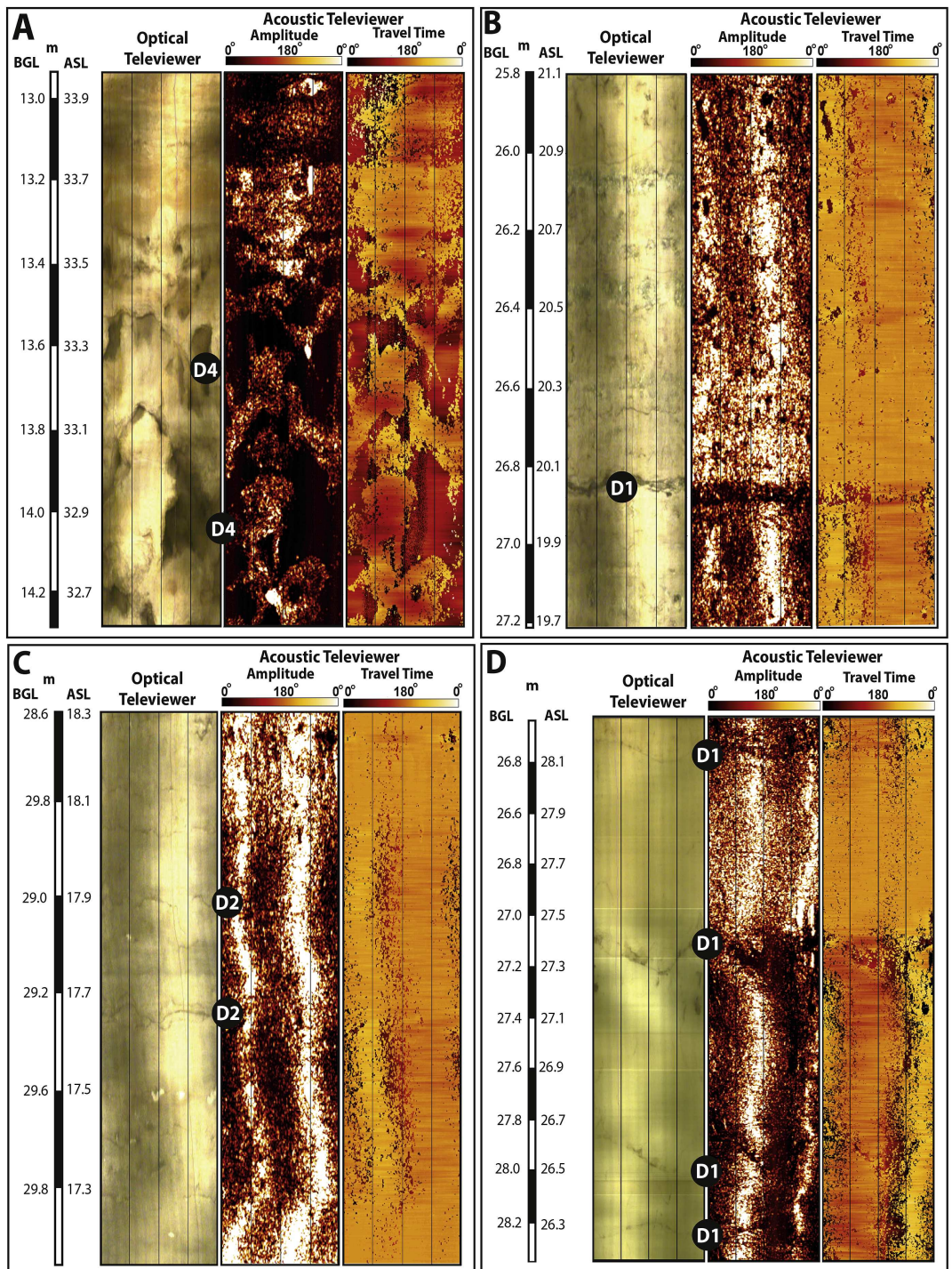


Figure 3

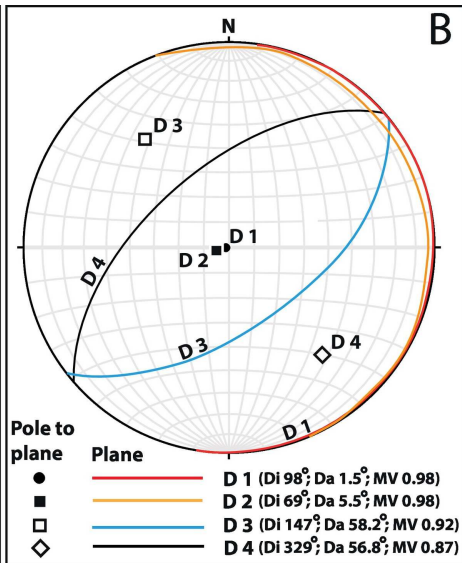
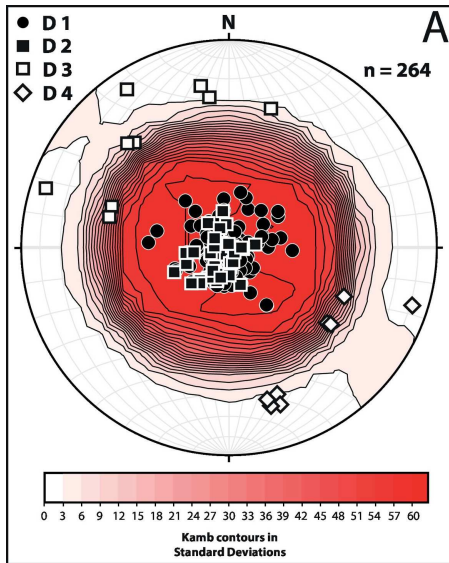


Figure 4

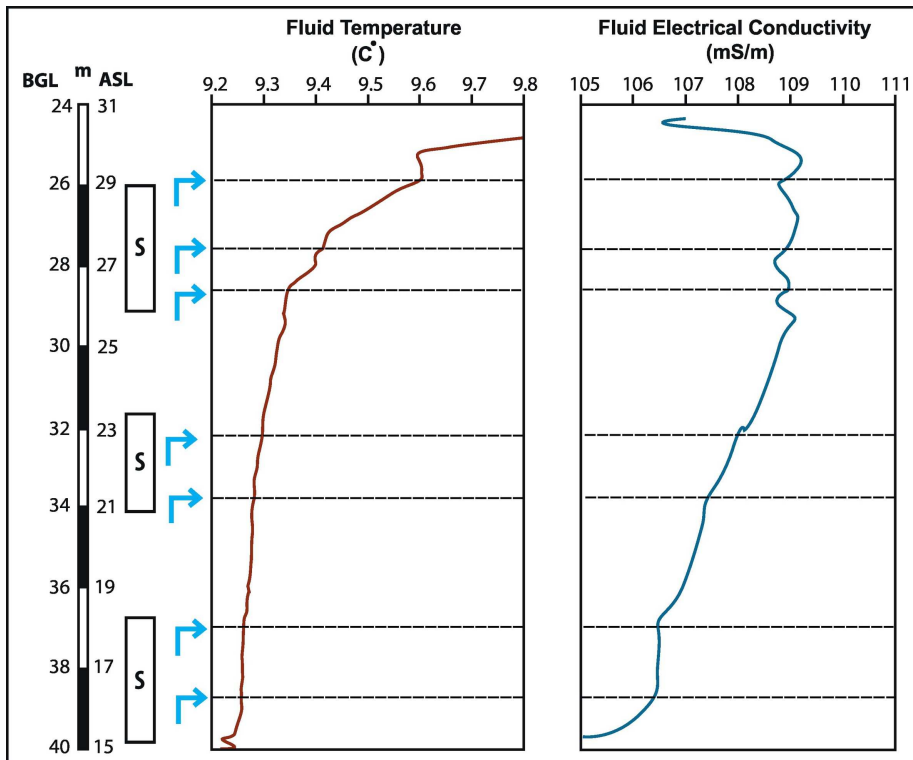


Figure 5

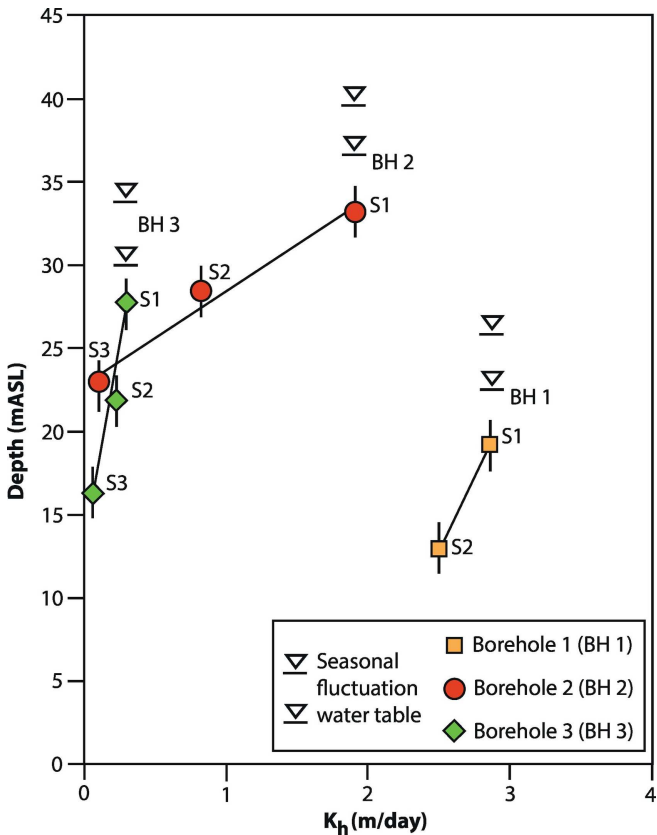


Figure 6

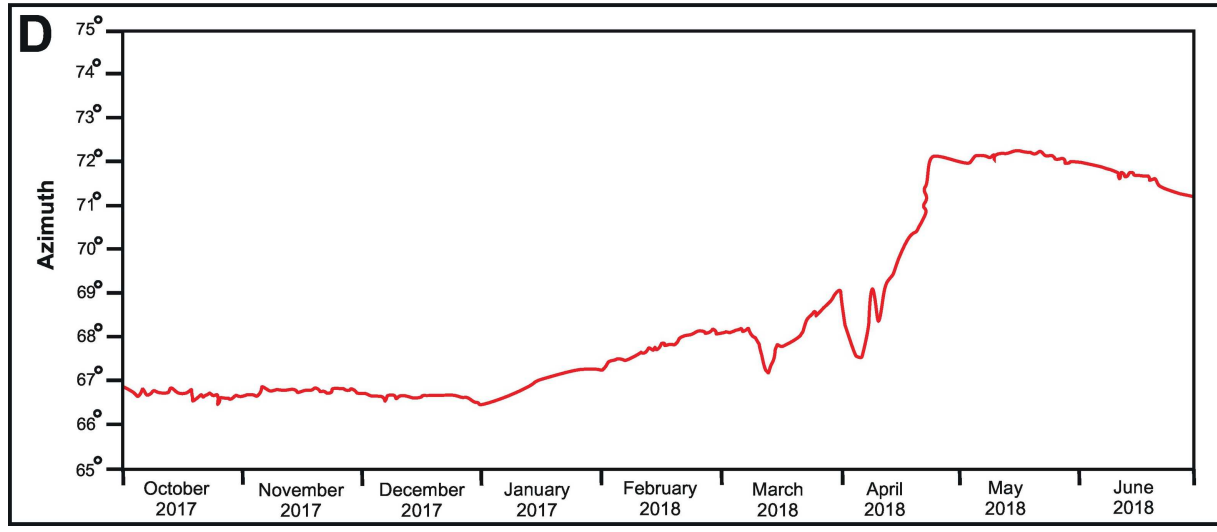
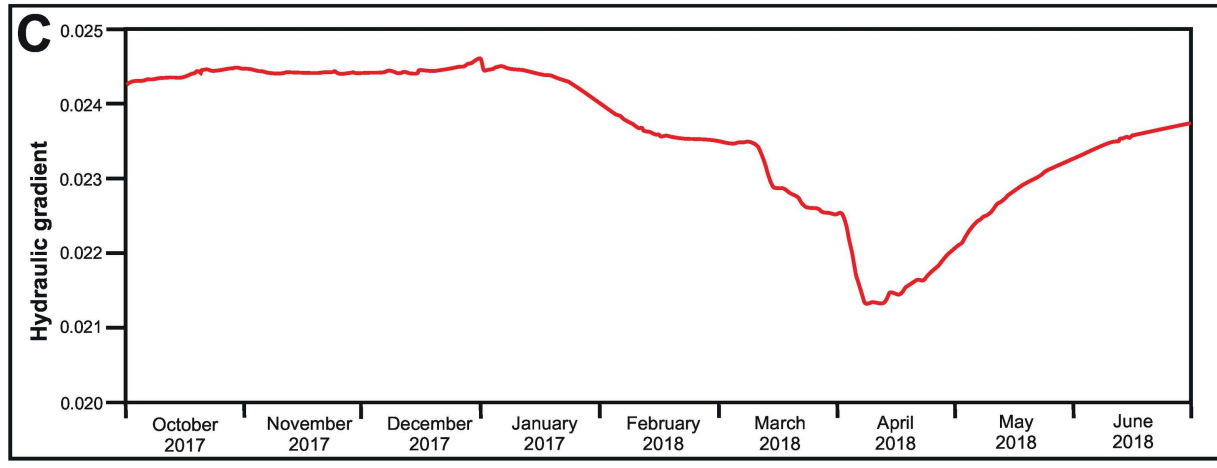
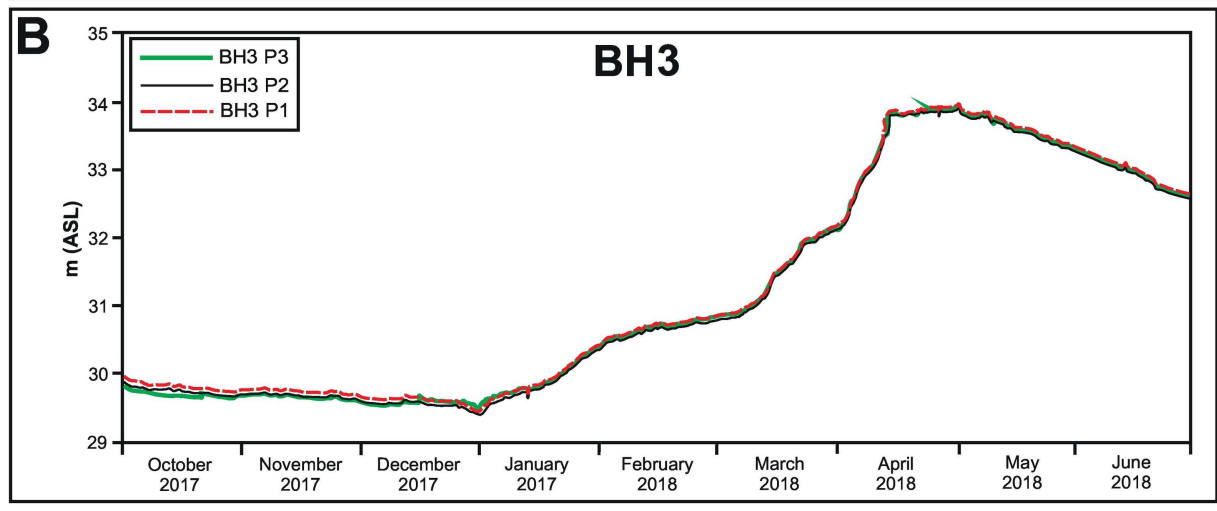
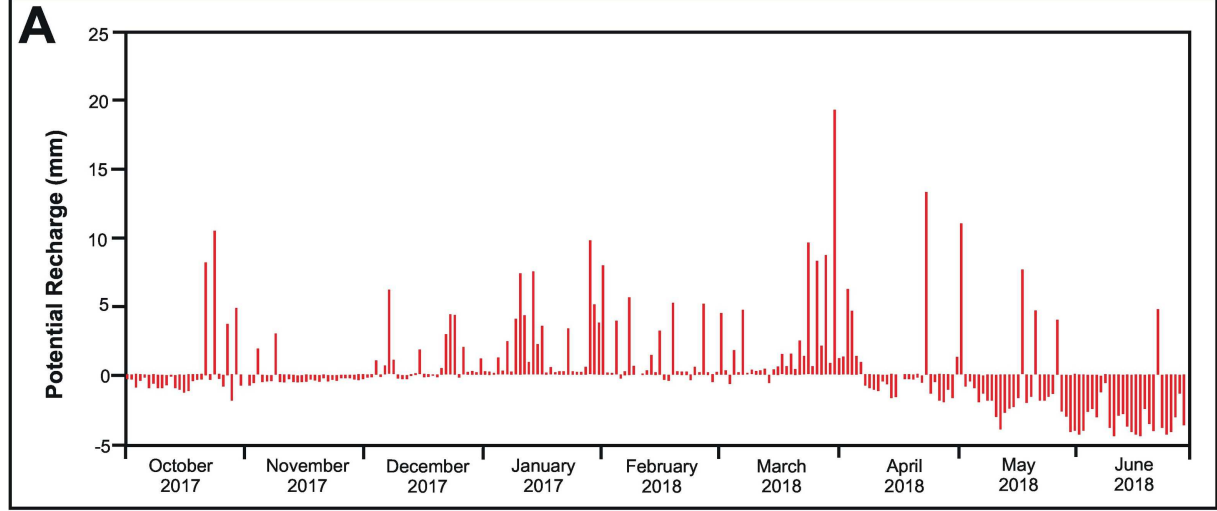


Figure 7

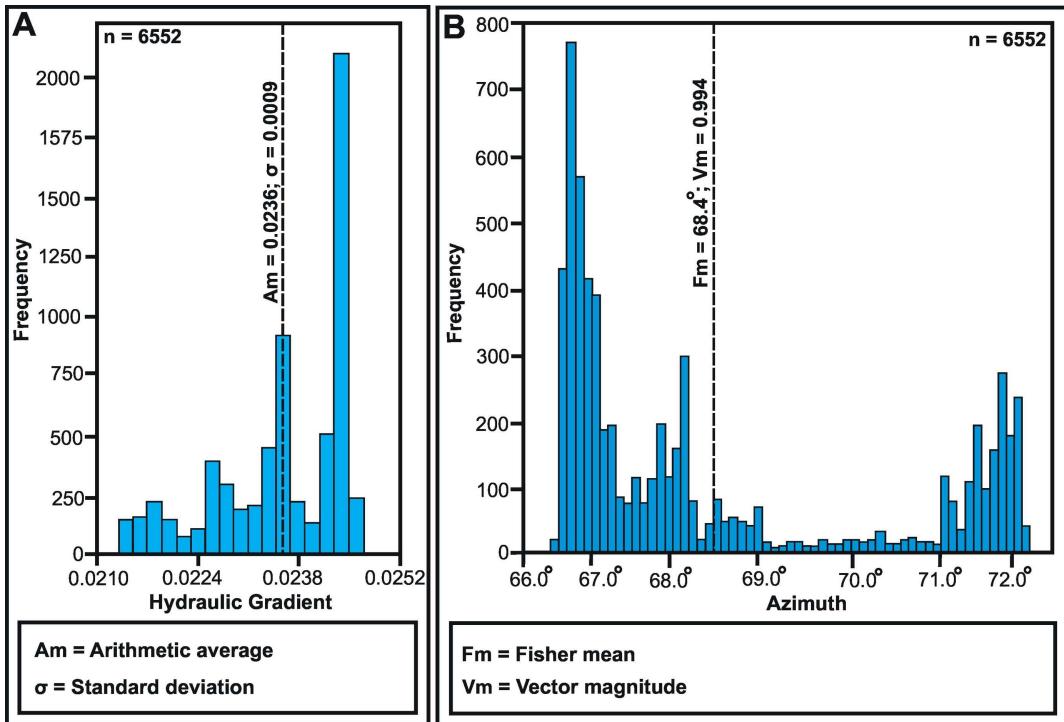


Figure 8

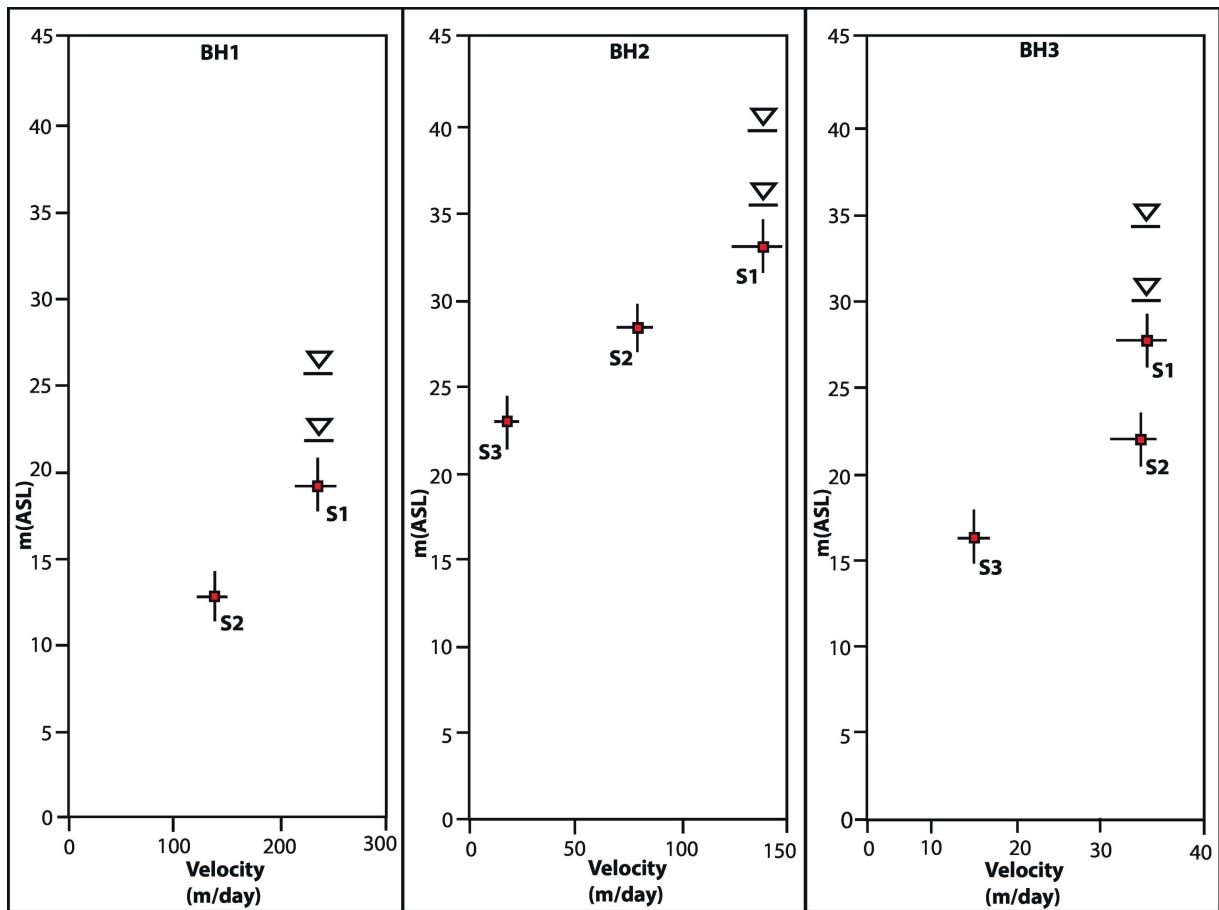


Figure 9

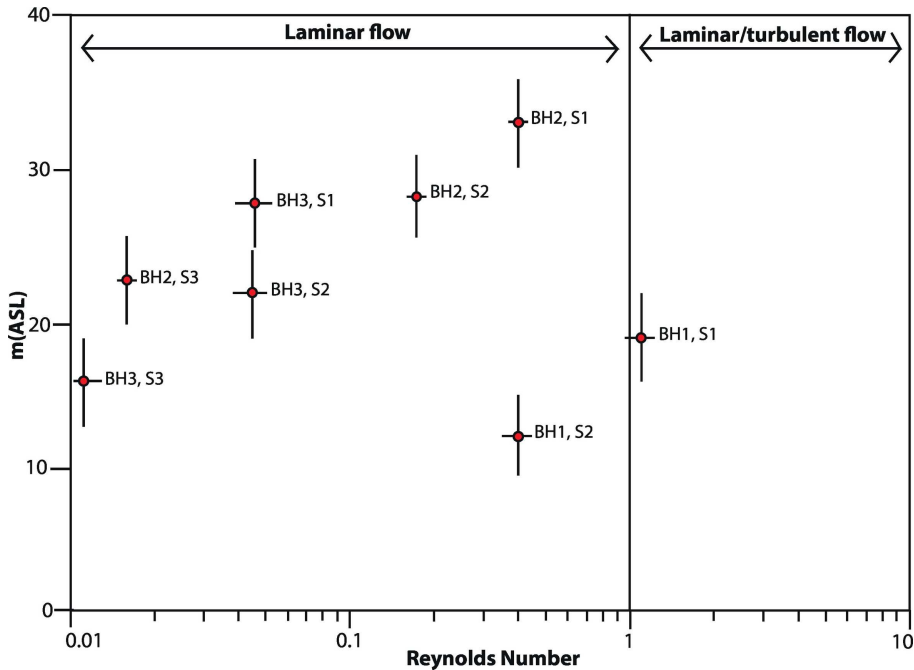


Figure 10

Fractured  
Carbonate Aquifer  
Critical Zone

Effective hydraulic aperture ( $b$ )  $\sim 10^{-1}$  mm  
Reynolds number ( $Re$ )  $\leq \sim 1$

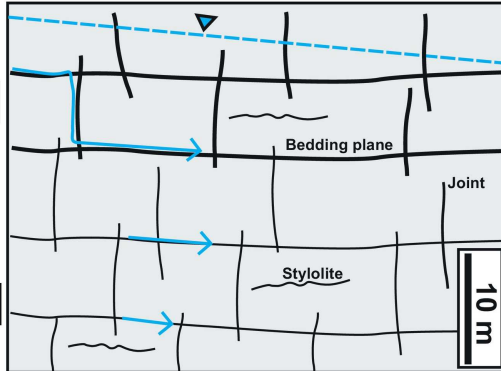
Non-faulted  
area

$K = 0.30 - 2.85$  m/day

$V = 33 - 242$  m/day

$K = 0.07 - 0.30$  m/day

$V = 10 - 33$  m/day



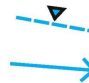
Key



Fracturing  
network  
- dissolution  
Fracturing  
network

$V$  = groundwater flow velocity

$K$  = hydraulic conductivity



Piezometric  
surface

Groundwater  
flow

Figure 11